On climate and abyssal circulation in the Atlantic Ocean during late Pliocene marine isotope stage M2, ~3.3 million years ago

Nicola Kirby[1,2], Ian Bailey*[3], David C. Lang[1], Anieke Brombacher[1], Thomas B. Chalk[1], Rebecca L. Parker[3], Anya J. Crocker[1], Victoria E. Taylor[1], James A. Milton[1], Gavin L. Foster[1], Maureen E. Raymo[4], Dick Kroon[5], David B. Bell[5], Paul A. Wilson[1]

1. School of Ocean and Earth Science, University of Southampton, Waterfront Campus, National Oceanography Centre Southampton, European Way, Southampton SO14 3ZH, UK.

2. Now at: Earth Sciences, School of Geography, Earth and Environmental Sciences, University of Birmingham B15 2TT, UK.

3. Camborne School of Mines, College of Engineering, Mathematics & Physical Sciences, University of Exeter, Penryn Campus, Treliever Road, Penryn TR10 9FE, UK.

4. Columbia University, Lamont-Doherty Earth Observatory, P.O. Box 1000, 61 Route 9W, Palisades, NY 10964, USA.

5. School of GeoSciences, University of Edinburgh, Edinburgh EH9 3JW, UK

6. Centre for Environmental Policy, Weeks Building, 16-18 Prince's Gardens, Imperial College London South Kensington, London SW7 1NE, UK.

*corresponding author: njk883@student.bham.ac.uk

Abstract: Marine Isotope Stage (MIS) M2, 3.3 Ma, is an isolated cold stage punctuating the benthic oxygen isotope ($\delta^{18}O$) stratigraphy of the warm Piacenzian interval of the late Pliocene Epoch. The prominent (~0.65‰) $\delta^{18}O$ increase that defines MIS M2 has prompted debate over the extent to which it signals an early

prelude to the rhythmic extensive glaciations of the northern hemisphere that characterise the Quaternary and raised questions about the forcing mechanisms responsible. Recent work suggests that CO_2 storage in the deep Atlantic Ocean played an important role in these events but detailed reconstructions of deep ocean chemical stratification are needed to test this idea and competing hypotheses. Here we present new records of the Nd isotope composition of fish debris and $\delta^{13}C$ and B/Ca ratios of benthic foraminifera from the northwest and southeast Atlantic Ocean. Our novel geochemical data show that, in contrast to major Quaternary glaciations such as MIS 2 (~21 kyr) and MIS 100 (~2.52 Ma), the deep North Atlantic Ocean was weakly chemically stratified during MIS M2. We show that Southern Component Water incursion into the Atlantic Ocean was limited to the deep South Atlantic basin during MIS M2 and peaked well before (~10-15-kyr) the atmospheric CO_2 minimum. Our findings imply that the deep Atlantic Ocean was not the principle sink of CO_2 sequestered from the atmosphere during MIS M2, implicating a different CO_2 storage deep-water reservoir mechanism, presumably Southern Component Water incursion into the Pacific Ocean. Weak chemical stratification in the deep Atlantic Ocean during MIS M2 relative to MIS 100 and 2 suggests comparatively active Atlantic meridional overturning circulation. That suggestion is consistent with the warmth of the high latitude North Atlantic during MIS M2 – surface water temperatures cooled during M2 but only to Holocene values. Our findings may help to explain the paucity of evidence for extensive early glaciation of the northern hemisphere during M2 but leave open the possibility of ice sheet advance on Antarctica.

Key words: AABW; NADW; Atlantic circulation; Last Glacial; MIS 100; MIS M2; AMOC

1. Introduction

Much of the Pliocene Epoch is considered to have been warmer than the pre-industrial with peak atmospheric carbon dioxide (pCO_2) levels about as high as present (413 ppm in 2019; Seki et al., 2010; Dowsett et al., 2012; Haywood et al., 2013; Martinez-Boti et al., 2015; de la Vega et al., 2020). Many studies of Pliocene warmth over the past two decades have focused on the mid-Piacenzian warm period (mPWP, 3.264 to 3.025 Ma), the most recent interval of sustained warmth during this epoch (McClymont et al., 2020). However, just prior to this time there occurred a transient interval of high latitude cooling beginning around 3.5 Ma during Marine Isotope Stage (MIS) MG5 that culminated during MIS M2, 3.295 Ma (Prell, 1984; Keigwin, 1987; Haug and Tiedemann, 1998; Jansen et al., 2000; Lisiecki and Raymo, 2005).

One interpretation of MIS M2 is that it signals early extensive northern hemisphere (and therefore) bi-polar glaciation (De Schepper et al, 2009; De Schepper et al., 2013). Yet the magnitude and location of land ice growth during this cold stage is poorly documented – if there was a major glacial advance it is not even known whether it was concentrated in the northern or southern hemisphere (e.g., Prell, 1984; Maslin et al., 1998; Dwyer and Chandler, 2009; De Schepper et al., 2009; Naish et al., 2009; McKay et al., 2012; Gao et al., 2012; De Schepper et al., 2013; De Schepper et al., 2014; Brigham-Grette et al., 2013; Dolan et al., 2015). Estimates of global sea-level fall associated with full glacial conditions of MIS M2 range from ~ 10 m lower than the present day (Naish et al., 1997; Miller et al., 2012) to as much as 65 m lower (Dwyer and Chandler, 2009). If the larger sea-level fall estimates relative to modern are substantiated, MIS M2 may mark the first time during the Cenozoic when the seawater component of benthic $\delta^{18}O$ increase was controlled by ice sheet growth in

77 the northern hemisphere. Yet while there is firm evidence for glacial expansion on
78 Greenland, Svalbard and Iceland during M2, the same is not true of North America or
79 mainland Eurasia (De Schepper et al., 2014). Furthermore, numerical ice-sheet
80 modelling experiments, simulate only small ice caps in the northern hemisphere,
81 equivalent to ~12 m fall in sea level (msle) (Tan et al., 2017), twice the seawater
82 equivalent of the modern Greenland Ice Sheet but an order of magnitude smaller than
83 the fall associated with the major glaciation of the Last Glacial Maximum (Lambeck
84 et al., 2014).

85 A small M2 ice-sheet budget for the northern hemisphere is also implied by a
86 new detailed record of atmospheric CO_2 for late Pliocene which shows a marked
87 decline during MIS M2 (from ~420 to 310 ppm) but to concentrations unlikely to
88 have fallen below the threshold suggested (DeConto et al., 2008) to trigger extensive
89 northern hemisphere glaciation (de la Vega et al., 2020). Atmospheric CO_2 decline
90 during MIS M2 lags benthic $\delta^{18}O$ by ~10 kyr but is in-phase with possible evidence
91 for Southern Component Water (SCW) incursion into the deep mid-latitude North
92 Atlantic Ocean (Lang et al., 2016; de la Vega et al., 2020). These observations imply
93 that expansion of a CO_2-charged SCW reservoir in the deep Atlantic may have been
94 active more than 600-kyr before the onset of significant northern hemisphere
95 glaciation ~2.72 Ma (de la Vega et al., 2020). Yet, while Nd isotope and $\delta^{13}C$ records
96 from Integrated Ocean Drilling Program (IODP) Site U1313 (Fig. 1) suggest that
97 major incursions of SCW of last glacial-magnitude occurred at this site during large
98 Quaternary glacials at least from MIS 100, 2.52 Ma (Lang et al., 2014; 2016), those
99 records are insufficiently resolved for MIS M2 to provide a clear test of whether the
100 same is true for this older more enigmatic cold stage (Fig. 1a,b).

101 To shed new light on the role of the Atlantic Ocean in CO_2 decline during MIS

M2, we present a new high-resolution (suborbital-scale) assessment of changes in water-mass distribution at deep Northwest Atlantic Ocean IODP Site U1313 (Fig. 2) and deep Southeast Atlantic Ocean Drilling Program (ODP) Site 1267 (~4350 m depth; ~29˚S, Fig. 2). We apply the same multi-proxy approach shown to be effective for tracking water-mass distribution during the last glacial (e.g., Yu et al., 2008; Chalk et al., 2019), combining neodymium-isotope composition of fish debris as well as the carbon isotope and B/Ca composition of benthic foraminifera to trace water-mass properties. Our new records for MIS M2 show contrasting structure to that seen for MIS 100 and MIS 2, strongly suggesting that the water-mass structure of the deep Atlantic Ocean during MIS M2 was quite different to that of large Quaternary glacials. We compare our data to published records for MIS M2 and discuss the implications of our new findings for our understanding of late Pliocene climate.

2. Methods

2.1. Study sites, sampling and chronology

We document change in three water-mass tracers ($\delta^{13}C$ and B/Ca in benthic foraminiferal calcite and Nd isotopes in fish debris) for MIS M2 from the deep western North Atlantic (Site U1313; Fig. 2) and deep eastern South Atlantic (Site 1267; Fig. 2) and compare their amplitude of change to new and published records for MIS 100 (2.52 Ma) and MIS 2 (21 ka), large Quaternary glacials for which major SCW incursion into the deep North Atlantic is documented by characteristic $\delta^{13}C$-CO_3^{2-}-Nd isotope relationships (e.g., Oppo and Fairbanks, 1987; Raymo et al., 1987, 1990, 1992; Hodell and Venz, 1992; Yu et al., 2008; Lang et al., 2016; Chalk et al., 2019). Given the caveats that come with water-mass provenance proxies, we follow Lang et al. (2016) in placing most confidence in signals of change documented in all

three water-mass-proxy records. To produce our new data sets we: 1) increased the resolution of the Site U1313 fish debris Nd isotope record published by Lang et al. (2016) for MIS M2 and MIS 100 (from ~6-7 kyr to ~3.5 and 1 kyr, respectively), and 2) developed new suborbitally resolved records of fish debris Nd isotopes and benthic foraminiferal B/Ca ratios and $\delta^{13}C$ for MIS M2 (3.24-3.33 Ma), 100 (2.5-2.55 Ma) and the last glacial-Holocene (0-40 ka) from Site 1267.

2.1.1. IODP Site U1313

IODP Site U1313 (41˚N, 32.4˚W, 3426 m depth, Fig. 2) constitutes a re-occupation of Deep Sea Drilling Project (DSDP) Site 607, a benchmark site for monitoring North Atlantic Deep Water (NADW) production during the Plio-Pleistocene (e.g., Ruddiman et al., 1989; Raymo et al., 1990, 1992; Raymo et al., 2004). Today, Site U1313 is bathed by 100% lower NADW. To increase the resolution of the previously published fish debris Nd isotope record for Site U1313 spanning MIS M2 and MIS 100, we analysed 14 additional samples from the shipboard primary splice (between 152.48-154.38 mcd; Expedition 306 Scientists, 2006) and 42 samples from the shipboard secondary splice (between 118.74-121.39 mcd; Expedition 306 Scientists, 2006). The age model for our MIS M2 record is based on retuning the Site U1313 benthic $\delta^{18}O$ stratigraphy (Bolton et al., 2010) to the LR04 stack (Lisiecki and Raymo, 2005) (Supplementary Information Section S2). To improve the age model for the Site U1313 stratigraphy spanning MIS 100 (which was previously based on assigning ages from the primary splice to the secondary splice stratigraphy by correlating between the two using shipboard-derived sediment colour reflectance data; Lang et al., 2016), we generated a new suborbitally resolved benthic foraminiferal $\delta^{18}O$ record (at on average ~1 kyr) between 118.64-122.44 mcd from the secondary

152 splice, which we subsequently tuned to the LR04 stack (Supplementary Information
153 Section S2).
154
155 2.1.2. ODP Site 1267
156 ODP Site 1267 (29˚S, 2˚E at 4350 m depth; Fig. 2) sits in the Angola Basin in the
157 Southeast Atlantic and monitors bottom-water conditions at the base of the northern
158 face of Walvis Ridge. Today Site 1267 is bathed by Lower Deep Water (LDW), a
159 mixture of 70-80% North Atlantic Deep Water (NADW) and 20-30% Antarctic
160 Bottom Water (AABW) sourced from the western Atlantic via the equatorial
161 Romanche and Chain Fracture zones and mixed vertically in the Angola Basin
162 downstream of these entry points (Fig. 2; Mercier and Morin, 1997; Arhan et al.,
163 2003). The Rio de Janeiro and Rio Grande Fracture zones, which cut the Mid-
164 Atlantic Ridge at 4000 m or greater depth at 21˚S and 26˚S, respectively, also funnel
165 AABW from the western South Atlantic Brazil Basin into the Angola Basin (Fig. 2;
166 Mercier et al., 2000). Together with two other passages below 4000 m in the southern
167 part of the Walvis Ridge near 36˚S 7˚W (the Walvis Passage) and 30˚S 2˚W (Connary
168 and Ewing, 1974), these fracture zones are the only pathways for AABW to reach Site
169 1267 (Fig. 2). During late Pleistocene glacials this site was more influenced by
170 AABW (with its relatively low $\delta^{13}C$, radiogenic Nd isotope and low carbonate ion
171 signature) because the interface between AABW and overlying NADW shoaled and
172 moved equatorward allowing more southern source deep water to enter the basin via
173 these fracture zones (Yu et al., 2008; Chalk et al., 2019; Farmer et al., 2019;
174 Pöppelmeier et al., 2020). The more southerly location (by ~70˚ of latitude) and
175 greater depth (by ~900 m) of Site 1267 relative to Site U1313 allows us to investigate

changes in the extent of SCW incursion northwards and shoaling of its interface with Northern Component Water (NCW) during MIS 2, 100 and M2.

To develop new records of Nd isotopes from fish debris and benthic foraminiferal B/Ca ratios from Site 1267 for MIS M2, MIS 100 and the last glacial-Holocene we analysed 89 samples taken from the shipboard primary splice between 0-0.34 mcd, 29.4-29.95 mcd and 40.27-41.42 mcd (41 of which were originally used to generate the published benthic $\delta^{18}O$ and $\delta^{13}C$ stratigraphies for Site 1267; Bell et al., 2014). The published age model for this site is based on alignment of a stack of Site 1267 and 1264 benthic $\delta^{18}O$ data for the past ~3.6 Ma to the LR04 (Bell et al., 2014). To improve this age model for MIS M2 and the last glacial-Holocene, we supplemented the previously published benthic $\delta^{18}O$ stratigraphy for Site 1267 by generating new $\delta^{18}O$ data between 0-0.34 mcd (n = 16) and 40.27-41.22 mcd (n = 50) and tuned the new resultant stratigraphies to the LR04 (Supplementary Information Section S2).

2.2. Stable isotope preparation and analysis

To generate new benthic foraminiferal stable isotope data ($\delta^{18}O$ and $\delta^{13}C$) for our target intervals, individual tests of the epifaunal species *Cibicidoides wuellerstorfi* (typically n>8) were picked from the 150-400 μm size fraction in 66 samples from Site 1267 (the same samples used to generate Nd isotope data for MIS M2, MIS 100 and the last glacial-Holocene) and from the 212-500 μm fraction in 73 samples from the secondary splice of Site U1313 (typically >8 tests per sample, the same samples used to generate Nd isotope data for MIS 100). After drying, picked individuals were cracked open and ultrasonically cleaned in methanol. This was done to remove adhering clays and any low $\delta^{18}O$ clay infilling before a homogenised aliquot was

transferred to reaction vials and analysed using a Thermo Finnigan MAT 253 dual inlet mass spectrometer equipped with a Kiel IV Carbonate Device at NOCS, University of Southampton. Data were calibrated using a two-point calibration to standards NBS 18 and 19. We also measured an internal standard (GS1) in each run as a quality control measure that yielded an analytical precision of 0.08‰ for $\delta^{18}O$ and 0.02‰ for $\delta^{13}C$ (at 2 s.d.) during the study period. Results are reported relative to the Vienna Peedee belemnite (VPDB) standard. Where the samples picked for stable isotope analysis were also used to generate benthic B/Ca data (e.g., from Site 1267, n = 56), the tests of the picked foraminifera were gently broken open and mixed before being split into two aliquots.

2.3. Nd-isotope preparation and analysis

The local Nd-isotope composition of bottom-water is reliably preserved in fossilised fish tooth, bone and scale hydroxyfluorapatite (henceforth fish debris) during early stage diagenesis, and is resistant to alteration on multi-million year timescales (Martin and Scher, 2004). To develop new Nd isotope datasets, we hand-picked ~50-200 mg of fish debris (10 to 30 pieces of bones and teeth) from the >150 μm fraction of Site U1313 samples and from the >38 μm fraction of Site 1267 samples. Fish debris was cleaned with two steps of ultrasonication in methanol, followed by three steps in Milli-Q 18.2 MΩ·cm water. Organic material was removed by bathing each sample in a buffered oxidising solution (1% H_2O_2 – 0.1M NH_4OH) at 80°C for 30 minutes, and sonicated for 30 seconds every 10 minutes. Finally, a weak-acid (0.001M HNO_3) polish was applied to ensure removal of any reabsorbed contaminants before samples were dissolved in 0.1ml 1.75M HCl.

Pure samples of Nd were extracted from our dissolved samples using a two-stage column procedure. First the rare earth element (REE) fraction was separated using Eichrom TRUspec resin, then Nd was separated from the REE fraction using Eichrom LNspec resin. The $^{143}Nd/^{144}Nd$ ratio was determined at the University of Southampton using a multi-collector inductively coupled plasma mass spectrometer (MC-ICP-MS, Thermo Scientific Neptune). Neodymium isotopic compositions were obtained using the method of Vance and Thirlwall (2002) through adjustment to a $^{146}Nd/^{144}Nd$ ratio of 0.7219 and a secondary normalization to $^{142}Nd/^{144}Nd = 1.141876$. Mass-bias corrected ratios were normalised to the given $^{143}Nd/^{144}Nd$ of the standard JNdi-1 (0.512115 (Tanaka et al., 2000)). Total procedural blanks averaged 35 pg during the analysis of our U1313 fish debris. Long-term replication of the JNdi-1 standard during this time yielded $^{143}Nd/^{144}Nd = 0.512118 \pm 0.000006$ (2 s.d.), giving an external reproducibility of 0.13 ε_{Nd} (2 s.d). Total procedural blanks averaged 39 pg during the analysis of our 1267 fish debris. Long-term replication of the JNdi-1 standard during this time yielded $^{143}Nd/^{144}Nd = 0.512116 \pm 0.00001$ (2 s.d.), giving an external reproducibility of 0.18 ε_{Nd} (2 s.d). In all cases we report the external uncertainty, unless the internal error is larger than the external error when we plot a combined error calculated as $\sqrt{(\text{external error}^2 + \text{internal error}^2)}$. All Nd isotope ratios are reported in epsilon notation (DePaolo and Wasserburg, 1976) as:

$$\varepsilon_{Nd} = \left[\frac{^{143}Nd/^{144}Nd_{sample}}{^{143}Nd/^{144}Nd_{CHUR}} - 1 \right] \times 10^4$$

Radiogenic in-growth of ^{143}Nd is corrected following (DePaolo and Wasserburg, 1976) using a crustal $^{147}Sm/^{144}Nd$ value of 0.125 (MacLeod et al., 2008). Such age-corrections are minor (<0.05 ε_{Nd} for our late Pliocene-earliest Pleistocene data, and

250 <0.0004 ε_{Nd} for last glacial-Holocene data), reflecting the young age of our samples
251 relative to the half-life of ^{147}Sm. We note that fish debris and authigenic Fe-Mn
252 oxyhydroxide $^{147}Sm/^{144}Nd$ typically varies within a narrow range (e.g., 0.121-0.136
253 (Martin et al., 2010)) and that our results are insensitive to the choice of value. The
254 sensitivity of our stated values to application of the range of $^{147}Sm/^{144}Nd$ = 0.121-
255 0.136 (Martin et al., 2010) is always <0.01 ε_{Nd}, which is negligible.
256
257 2.4 Fresh volcanic glass counts
258 The ε_{Nd} signal recorded by fish debris can be modified by partial dissolution of fresh
259 radiogenic basaltic volcanic glass by sediment pore waters post deposition (Du et al.,
260 2016). It has been suggested that young volcanic glass sourced from the nearby
261 Azores volcanic island eruptions may have influenced the ε_{Nd} signal recorded at
262 U1313 during the Holocene (Blaser et al., 2016). To evaluate whether porewater
263 volcanic glass dissolution may have played a role in the trends documented in our Site
264 U1313 ε_{Nd} data we determined the concentration of fresh volcanic glass (>63 μm g^{-1})
265 in 53 of the Site U1313 samples analysed in this study and by Lang et al. (2016) for
266 fish debris ε_{Nd} using a standard method (e.g., Bond and Lotti, 1995).
267 It has been suggested that increased inputs of detrital carbonate sourced from
268 the Canadian Shield (Hudson Bay) to Site U1313 during Heinrich events are
269 responsible for millennial-scale unradiogenic excursions in authigenic ε_{Nd} at this site
270 (e.g., Lang et al., 2016; Du et al., 2020). Yet, Heinrich layer deposition at Site U1313
271 was restricted to the past ~640 kyr (Naafs et al., 2014). Furthermore, IRD
272 accumulation rates at U1313 are extremely low during ambient glacial conditions
273 over the past ~3.3 Myr (Lang et al., 2014; Lang et al., 2016).
274

275 2.5 Benthic foraminiferal boron/calcium ratios

276 Between 8 and 12 *C. wuellerstorfi* tests (212-500 μm) were cleaned for trace metal
277 analysis from 56 samples from Site 1267 spanning MIS M2, MIS 100 and the last
278 glacial-Holocene following Chalk et al. (2019). Foraminiferal tests were cracked open
279 and ultrasonicated several times in Milli-Q 18.2 MΩ·cm water to remove clay
280 materials. Samples were then oxidatively cleaned in a NH_3OH buffered 1% hydrogen
281 peroxide solution before a 0.0005M weak acid leach was applied to remove adsorbed
282 cations. Finally, samples were dissolved in ~0.075 M nitric acid. The above steps
283 were all undertaken in the boron-free clean laboratory at the University of
284 Southampton. Element ratios were measured using a ThermoFisher Scientific Element
285 2XR-ICPMS at Southampton, using the protocol described by Rae et al. (2011)
286 employing matrix-matched in-house standards and a variety of consistency standards
287 to ensure reproducibility. Samples were screened for clay contamination using Al/Ca
288 and other contaminant ratios (e.g., Ba/Ca, Fe/Ca), with samples Al/Ca > 200
289 μmol/mol excluded from this study (n = 4 out of 56). Long-term reproducibility for
290 B/Ca during this study was evaluated using consistency standards analysed during
291 each analytical session and within 4% at 2 s.d. (~2 mmol/mol). Carbonate ion
292 concentrations were calculated using a sensitivity of $\Delta[CO_2^{3-}]$ on B/Ca of 1.14 ±
293 0.048 for *C. wuellerstorfi* (Yu and Elderfield, 2007), and a $[CO_2^{3-}]_{sat}$ calculated from
294 modern local pressure, temperature and salinity (see Supplementary Information
295 Section S3). The influence of this assumption on the calculated $\Delta[CO_2^{3-}]$ is very
296 small (<0.5 umol/kg; Yu and Elderfield, 2007).

297

298 2.6 Water-mass geochemical end-members

299 We focus on relative change in water-mass composition between different glacials

300 rather than absolute changes but, nevertheless, consider the potential for change in
301 end-member compositions of NCW and SCW. To monitor the $\delta^{13}C$ of NCW during
302 our three target intervals, we use benthic $\delta^{13}C$ data from shallow northeast ODP Site
303 982 (1145 m water depth; Venz et al., 1999). The question of how best to monitor the
304 $\delta^{13}C$ of SCW is more contentious. Sequences recovered from areas ideally located to
305 monitor the end-member composition of SCW (e.g., in the Atlantic sector of the
306 Southern Ocean) are carbonate-poor. Because of this issue, one pioneering study used
307 benthic $\delta^{13}C$ from mid-latitude South Atlantic ODP Site 1090 (~3700 m water depth)
308 for this purpose for the Plio-Pleistocene (Venz and Hodell, 2002). We now know,
309 however that, today and in the past, Site 1090 is partially bathed by NCW (Pena and
310 Goldstein, 2014) making it ill-suited for this purpose. We therefore follow Raymo et
311 al. (1990) and Oppo et al. (1995) and use the $\delta^{13}C$ of Pacific deep water (equatorial
312 Pacific ODP Site 849 (3851 m water depth; Mix et al., 1995) as a conservative, albeit
313 aged, record of the end-member composition of SCW. However, we also compare
314 benthic $\delta^{13}C$ data from our study sites to the benthic $\delta^{13}C$ stratigraphy of Southwest
315 Pacific ODP Site 1123 (3290 m water depth, Fig. S1; Patterson et al., 2018), which is
316 bathed today by a mixture of Antarctic Bottom water and Lower Circumpolar Deep
317 Water. While its Plio-Pleistocene benthic $\delta^{13}C$ stratigraphy shows that the
318 composition of SCW bathing the deep Atlantic has changed over the period of our
319 study interval, it also confirms that marked differences persisted in the $\delta^{13}C$ of NCW
320 and SCW during cold stages over the past 3.6 Ma. The $\delta^{13}C$ of Site 1123 is thought to
321 have decreased from 3.6 Ma in response to increased carbon remineralisation in SCW
322 caused by Southern Ocean sea-ice expansion and a reduction in deep ocean
323 ventilation (Patterson et al., 2018).
324 Knowledge of the ε_{Nd} of NCW and SCW endmembers during the Plio-

Pleistocene, as well as the validity of using fish debris Nd isotope records to reconstruct water-mass mixing in the deep Atlantic over this time, is comprehensively discussed in Lang et al. (2016). Briefly, despite their extremely slow precipitation rates, our best source of information on the evolution of the Nd isotope composition of NCW and SCW during the Plio-Pleistocene arguably remains the ε_{Nd} of Fe-Mn crusts. To estimate the ε_{Nd} of these water-masses during MIS M2 and MIS 100, we therefore followed Lang et al. (2016) and took the average value of all published northwest Atlantic Fe-Mn crust ε_{Nd} data and their 2 s.d. that span ~3.3-2.4 Ma (from BM1969.05, ALV539 2-1 and TR079-D14; see supplementary Table S7). For the last glacial-Holocene, following the approach of Piotrowski et al. (2005), NCW ε_{Nd} was defined as the average of previously published Holocene data (<14 ka, MIS 2/1 boundary as defined by Lisiecki and Raymo (2005)) and their 2 s.d. for Site U1313 (Lang et al., 2016). We also define the SCW end-member ε_{Nd} for all our time target intervals using the ε_{Nd} crust record D18-1 from the Indian Ocean Sector of the Southern Ocean (see supplementary Table S7).

Traditionally, near-consistency in the NCW and SCW end members on orbital timescales is widely assumed in Nd isotope studies of water-mass mixing (e.g., Piotrowski et al., 2005; Böhm et al., 2014; Howe et al., 2016; Lippold et al., 2016). Yet, recently published records (Wilson et al., 2014; Roberts and Piotrowski, 2015; Hu et al., 2016; Pöppelmeier et al., 2018; 2019a; Pöppelmeier et al., 2019b; Zhao et al., 2019; Huang et al., 2020) and numerical modelling studies (e.g., Gu et al., 2019; Du et al., 2020), raise the possibility that NCW and SCW ε_{Nd} may have changed, at least, between the Last Glacial Maximum and the Holocene. In particular, the ε_{Nd} of cores from the New England slope at ~1800 m depth (KNR198), a region that should have been bathed in NCW throughout the Last Glacial Maximum-Holocene, suggest

that the preformed composition of NCW may have been up to ~4 ε-units more positive than today during the Last Glacial Maximum (Zhao et al., 2019). In this revised framework, radiogenic excursions in ε_{Nd} in the deep North Atlantic during the Last Glacial Maximum may reflect changes in the end-member composition of NCW rather than SCW incursion (Zhao et al., 2019; Pöpplemeir et al., 2020; Du et al., 2020). One interpretation of these signals is that higher ε_{Nd} in the deep North Atlantic during the Last Glacial Maximum (by ~3.5 ε-units, e.g., Böhm et al., 2015; Lang et al., 2016) reflects a reduction in chemical weathering of old unradiogenic cratonic rocks on Canada and Greenland under extensive northern hemisphere ice-sheets and that, when end-member changes are taken into account, the deep North Atlantic remained bathed in near 100% NCW with northward expansion of SCW limited to the deep South Atlantic (Zhao et al, 2019; Pöppelmeier et al., 2020).

The plausibility of temporal variations in NCW ε_{Nd} being driven by chemical weathering has recently been challenged by Du et al. (2020) from a tracer budget perspective. The notion that the extent of chemical weathering on North America controls the ε_{Nd} of NCW is also challenged by North Atlantic crust records which demonstrate that, as ice-sheet coverage of high northern latitude Archean and Proterozoic cratons increased over the past 3.3 Myr, the long-term Nd isotope composition of NCW has decreased (Burton et al., 1999; Vance and Burton, 1999; Reynolds et al., 2004). A dominant role for chemical weathering is also hard to reconcile with the fact that Site U1313 ε_{Nd} appears to vary in phase with southern (not northern) hemisphere insolation, especially prior to 2.7 Ma (Supplementary Figure S6). An alternative interpretation of the high ε_{Nd} values in the North Atlantic during the Last Glacial Maximum is that they reflect a reduction in the contribution to NCW of unradiogenic Labrador Seawater (Hillaire-Marcel et al., 2001a; 2001b) and a shift

375 in the location and mode of NCW formation to south of Iceland (Sarnthein et al.,
376 1994) where its preformed composition is made more positive by 'bottom-up' non-
377 conservative processes (i.e., partial dissolution of radiogenic authigenic (volcanic)
378 phases) enhanced by a more sluggish glacial circulation (Du et al., 2020). Given
379 these uncertainties, we proceed with caution herein, assuming near-consistency in Nd
380 end-members on orbital timescales (the traditional interpretive framework), but also
381 discuss the implications of this revised framework.
382
383 **3 Results and Discussion**
384 **3.1. Nd isotopes and B/Ca ratios**
385 In Figures 3 and 4 we integrate new and published data to present high resolution
386 records of fish debris-derived ε_{Nd} and B/Ca and $\delta^{13}C$ in benthic foraminiferal calcite
387 for the deep Atlantic Ocean during MIS M2, ~3.3 Ma, MIS 100, ~2.52 Ma, and the
388 last glacial-Holocene, ~40-0 ka. Our reconstruction of ε_{Nd} and $[CO_3^{2-}]$ in bottom-
389 waters bathing Site 1267 during the latest Holocene (averages = ~ –10.7±0.2 and
390 93±10 μmol kg^{-1}) are strikingly similar to those reported for LDW bathing Walvis
391 Ridge in the Angola Basin today (ε_{Nd} = –10.6±0.7; 30˚S 1˚W, 4675 m water depth
392 (Jeandel, 1993) and $[CO_3^{2-}]$ = ~100 μmol kg^{-1} (Lauvset et al., 2016)) strongly
393 suggesting that our data from this site faithfully track changes in deep water-mass
394 mixing in the Angola Basin (also see Supplementary Information Section 5).
395 The magnitude of peak interglacial-full glacial change in $[CO_3^{2-}]$, ε_{Nd} and
396 benthic $\delta^{13}C$ at Site 1267 is comparable between all three of our studied time
397 windows (with average IG-G change of ~10-22 μmol kg^{-1}, ~0.7-1.9 ε-units and ~0.4-
398 0.5 ‰, respectively; data in red in Fig. 3d-l; Tab. 1). The new highly resolved Nd
399 isotope record from Site U1313 for MIS 100 confirms the last glacial-magnitude shift

in ε_{Nd} (~1.85 for peak interglacial to full glacial; data in black and grey in Fig. 3h; Tab. 1) inferred from a less well resolved record (data in grey in Fig. 3h; Lang et al., 2016). The new high-resolution record for MIS M2 at Site U1313 also shows that, while there is a prominent short-term maximum in ε_{Nd} during the early glacial phase of M2 (~3.305 Ma, labelled EG in Fig. 3i), by the time full glacial (FG) conditions are reached at this site, ε_{Nd} is only ~0.7 ε-units higher on average than during the preceding interglacial MIS MG1 (Tab. 1). No analogous early glacial short-term structure in ε_{Nd} is documented in the corresponding benthic $\delta^{13}C$ record for MIS M2 (compare data in grey in Fig. 3i to 3l). The magnitude of change in benthic $\delta^{13}C$ at Site U1313 is small throughout MIS M2 (average IG-G change of only ~0.2 ‰) relative to both MIS 100 (average IG-G change of ~0.75 ‰) and the last glacial-Holocene (average IG-G change of ~0.55 ‰).

3.2. Deep Atlantic Ocean structure during the Last Glacial-Holocene

Our data reveal distinct geochemical differences between bottom waters at Site 1267 (today bathed in 70-80% lower NADW) and Site U1313 (today bathed in 100% lower NADW) in ε_{Nd}, benthic $\delta^{13}C$ and $[CO_3^{2-}]$ over the past ~10 kyr (>+2 ε-units, -0.3 ‰ and ~–20 µmol kg^{-1}, respectively) (Fig. 4a, d, j). These observations demonstrate that SCW influenced bottom-waters bathing the northern flank of Walvis Ridge throughout the Holocene. Our $[CO_3^{2-}]$ estimates for MIS 2 at Site 1267 (data in red in Fig. 4a) are comparable to those reported for the deep northeast North Atlantic (e.g., IODP Site U1308 at 51˚N and ~3800 m depth, data in dark blue in Fig. 4a) but they are ~80 µmol kg^{-1} lower than those estimated for the mid-depth northeast North Atlantic (e.g., ODP Site 980 at 55˚N and ~2170 m depth, data in green in Fig. 4a). The new $[CO_3^{2-}]$ estimates from Site 1267 therefore also show that the pronounced

425 carbonate-system depth-stratification reconstructed (e.g., by Yu et al., 2008; Chalk et
426 al., 2019) for the eastern Atlantic basin during the last glacial (compare [CO_3^{2-}] 980
427 data in green with U1308 and 1267 data in dark blue and red, respectively, in Fig. 4a)
428 probably extended southwards to Walvis Ridge (at ~30˚S). The new data are also
429 consistent with the suggestion (Chalk et al., 2019) that the dissolved inorganic carbon
430 (DIC) contents of the deep eastern Atlantic, at depths >3800 m, may be larger than
431 those of contemporaneous deep waters in the western Atlantic (compare data in red,
432 dark blue and black in Fig. 4a).

433 The simplest explanation for the radiogenic ε_{Nd}, low benthic $\delta^{13}C$ and low B/Ca
434 ratios in our MIS 2 datasets for Site 1267 is that they reflect an increased influence of
435 SCW on deep-waters bathing Walvis Ridge in the Angola Basin relative to the
436 Holocene. This explanation holds true even when recent assumptions about potential
437 changes in NCW and SCW during the Last Glacial Maximum (e.g., Zhao et al., 2019;
438 Pöppelmeier et al., 2020) are considered because our Site 1267 ε_{Nd} are still more
439 radiogenic than those recorded at Site KNR198, a recently proposed record of
440 preformed NCW for the Last Glacial Maximum (Zhao et al., 2019); Fig. 4d). In this
441 explanation, the pathway for SCW to the Angola Basin is the Romanche Fracture
442 zone, which today provides an equatorial passageway for SCW to this basin down to
443 4350 m (labelled RFZ in Fig. 2). This fracture zone was recently invoked as a route
444 for SCW during MIS 2 and used to explain low [CO_3^{2-}] in bottom waters bathing the
445 northeast North Atlantic (Site U1308 at 51˚N) during this time (Chalk et al., 2019).
446 As in the modern, the Vema Fracture Zone (VFZ), situated further north but in even
447 deeper water (~5000 m) (Fig. 2; Demidov et al., 2006) provides an even more
448 effective conduit for SCW flow to reach the northeast North Atlantic during Plio-
449 Pleistocene glacials. The deeper VFZ may help explain why bottom waters bathing

Site U1308 during the Last Glacial Maximum have lower [CO_3^{2-}] than those bathing Site 1267.

Today, the [CO_3^{2-}] of deep-waters can be used as a quasi-conservative tracer of water-mass source, but this may not have been the case during MIS 2. A variety of processes unrelated to water-mass mixing can modify the [CO_3^{2-}] of the ocean (e.g., air-sea exchange, alkalinity change and biological processes), but given that [CO_3^{2-}] will react differently to these processes compared to $\delta^{13}C$, paired [CO_3^{2-}]-$\delta^{13}C$ data can be used to determine whether changes in the former reflect changes in water-mass structure or non-conservative processes (e.g., Yu et al. 2008; Chalk et al., 2019). The trend of paired [CO_3^{2-}]-$\delta^{13}C$ data from Site U1308 for the last glacial and Holocene approximates best to a trend line indicative of CO_2 influx (e.g., of ocean uptake of carbon), indicating carbonate system proxy data can be used at this site as a quasi-conservative tracer of SCW-NCW mixing (small black filled and hollow circles in Fig. 5a). By contrast, the gradients of paired [CO_3^{2-}]-$\delta^{13}C$ data from sites 1267 and U1313 for the same time interval in $\delta^{13}C$-[CO_3^{2-}] space is significantly steeper (solid and hollow green and red circles in Fig. 5a) and better approximate the slope of the 'biology line' of Yu et al. (2008). This observation indicates that carbon remineralization may have contributed to the paired low $\delta^{13}C$ and [CO_3^{2-}] values at sites 1267 and U1313 during MIS 2 (by decreasing the $\delta^{13}C$ of DIC bathing 1267 and U1313 beyond that anticipated from linear mixing of SCW-NCW alone). Nevertheless, an increase in the contribution of SCW to these two sites relative to the Holocene is indicated by our ε_{Nd} records (Fig. 4d).

Dense Norwegian-Greenland Sea (NGS) overflows are proposed to contribute to the deep waters bathing Walvis Ridge throughout much of the Pleistocene (Bell et al., 2014; 2015). This suggestion invokes a deep Eastern Atlantic route for this water-

475 mass to the Angola Basin. This possibility cannot be ruled out for our study intervals
476 based on our ε_{Nd} data alone because today both Nordic Sea overflows and AABW
477 share a radiogenic ε_{Nd} signature (of ~ –7 to –9; Crocker et al., 2016). Yet $[CO_3^{2-}]$ is
478 markedly higher for modern NGS overflow water (>115 μmol kg^{-1}) than for SCW
479 (~85 μmol kg^{-1}) and this contrast would have been greater during the Last Glacial
480 Maximum than today (Yu et al., 2008; Crocker et al., 2016). Thus, it is unlikely that
481 the radiogenic (ε_{Nd} = –9, Fig. 4d-e) and $[CO_3^{2-}]$ low (= ~80±10 μmol kg^{-1}, Fig. 4a-b)
482 deep-waters bathing Site 1267 during the MIS 2 and MIS 100 were composed of
483 dense overflow waters sourced directly from the NGS via an abyssal eastern basin
484 route. This is a robust interpretation even if their composition was overprinted en
485 route by extensive biological remineralization of carbon.
486
487 **3.3. Deep Atlantic Ocean structure during MIS M2 and 100**
488 The consistency in the amplitude of IG-G change in all three water-mass proxies at
489 Site 1267 during all three of our target time slices (Tab. 1) suggests that the
490 oceanographic response to MIS M2, MIS 100 and MIS 2 in the deep South Atlantic
491 was similar across all three glacials, i.e., all proxies reflect an increase in the influence
492 of SCW. In contrast, IG-G changes in $\delta^{13}C$ and ε_{Nd} at Site U1313 suggest a smaller
493 contribution of SCW to deep waters bathing this shallower more northerly situated
494 site during MIS M2 than during MIS 100 and MIS 2 (Tab. 1).
495 The validity of this conclusion depends on there not being major changes in the
496 offset between the end-member compositions of NCW and SCW during these times.
497 A last-glacial-Holocene-like change in ε_{Nd} at Site 1267 during MIS M2 and MIS 100
498 could be artificially produced by a more positive SCW ε_{Nd} during these cold stages
499 relative to MIS 2. Because SCW is a mixture of relatively unradiogenic Atlantic and

500 radiogenic Pacific waters (Stichel et al., 2012) a more positive SCW could arise in
501 two ways. First, if the composition and mixing contribution of the Pacific end-
502 member to SCW remained similar during our three studied glacials, a more positive
503 NCW would lead to a more positive SCW when it mixes with Pacific deep waters in
504 the Southern Ocean. Second, SCW could become more positive if NCW makes a
505 smaller contribution to SCW due to a reduction in the southward advection rate of
506 North Atlantic deep waters. Based on the available crust data (Frank et al., 2002), it is
507 reasonable to assume that the ε_{Nd} composition of the Pacific end-member remained
508 stable during our study intervals, but the Nd isotope composition of NCW did not
509 (compare red and blue horizontal bars in Fig. 4d-f). Both the crust records and Site
510 U1313 ε_{Nd} illustrate that NCW was ~1 ε-unit more radiogenic during the late Pliocene
511 than it was during the late Pleistocene (Fig. 4d-f). Yet, a relatively radiogenic NCW
512 during MIS 100 and MIS M2 would not have changed the gradient in ε_{Nd} between
513 NCW-SCW during these cold stages relative to MIS 2 because it would also have
514 made SCW more radiogenic. We can also rule out the possibility that a reduction in
515 the southward advection rate of NCW relative to MIS 2 could explain the existence of
516 a last-glacial-Holocene-like change in ε_{Nd} at Site 1267 during MIS M2 and MIS 100
517 because it is unlikely that Atlantic Meridional Overturning Circulation (AMOC)
518 weakening was greater during late Pliocene and earliest Pleistocene cold stages than
519 during MIS 2.

520 Our interpretations of relative changes in our water-mass proxy data are
521 supported by a comparison between the benthic $\delta^{13}C$ data from our study sites and the
522 well-constrained $\delta^{13}C$-based estimates of NCW and SCW end members (Fig. 4j-l). A
523 comparison of benthic $\delta^{13}C$ values at Site 1267 to those at Site 982 (the NCW end-
524 member) reveals that there was an increased contribution of SCW bathing Walvis

525 Ridge for most of early- to mid-glacial M2 until ~3295 ka (compare data in red and
526 purple in Fig. 4l). While our knowledge of NCW and SCW ε_{Nd} during MIS M2 is less
527 certain, our Nd isotope data from this site record the same history of SCW incursion
528 during this cold stage as inferred from benthic $\delta^{13}C$ (compare data in red and orange
529 in Fig. 6d). In contrast, at Site U1313, benthic $\delta^{13}C$ values are comparable to those of
530 NCW throughout MIS M2 (compare data in black and purple in Fig. 4l). We infer
531 that, while SCW contributed significantly to the deep waters bathing Site 1267 during
532 this glacial at least until ~3295 ka, Site U1313 was mainly bathed by NCW during
533 MIS M2. We note the radiogenic spike in Nd during early MIS M2 (star in Fig. 4f)
534 but find no supporting evidence that it arises from water-mass mixing (see
535 supplementary information Section S6).
536
537 3.3.1 What would be the implication of changing ε_{Nd} end members for
538 our interpretation of MIS M2?
539 We have interpreted the history of deep Atlantic Ocean structure using the traditional
540 framework wherein the end-member ε_{Nd} compositions of NCW and SCW did not
541 change appreciably on glacial-interglacial timescales (e.g., Foster et al., 2007;
542 Piotrowski et al., 2005; Böhm et al., 2015; Howe et al., 2016). If major end-member
543 change in NCW occurred over the last glacial cycle (of ~+4 ε-units) then it is possible
544 that the deep North Atlantic remained bathed in near 100% NCW during the Last
545 Glacial Maximum and northward expansion of SCW was limited to the deep South
546 Atlantic (Zhao et al, 2019; Pöppelmeier et al., 2020). However, an absence of SCW in
547 the deep North Atlantic during the Last Glacial Cycle is hard to reconcile with the fact
548 that benthic $\delta^{18}O$ from, e.g., the Iberian Margin correlates so well with Antarctic
549 temperature (Shackleton et al., 2000). Nevertheless, in this scenario, the large

550 negative excursion recorded in North Atlantic benthic $\delta^{13}C$ records during the Last
551 Glacial Maximum is proposed to reflect enhanced remineralisation of carbon in deep-
552 waters (Howe et al., 2016) under a more sluggish (i.e., diminished AMOC) glacial
553 deep Atlantic circulation relative to modern (Böhm et al., 2015; Ng et al., 2018).
554 What would be the implication for our interpretation of MIS 100 and M2 if this
555 alternative framework is correct? There are two suggested mechanisms for NCW end-
556 member change. In the first case, change is driven by chemical weathering extent on
557 North America (Zhao et al., 2019; Pöppelmeier et al., 2020) such that deep North
558 Atlantic ε_{Nd} acts as a proxy of Plio-Pleistocene North American Ice Sheet extent. In
559 this case, the large radiogenic ε_{Nd} excursions during MIS 2 and MIS 100 at Site
560 U1313 (Lang et al., 2016; this study; Fig. 3g-h; Tab. 1) signal comparable reductions
561 in chemical weathering on North America and Greenland due to a similar spatial
562 configuration of ice-sheets on Canada and Greenland whereas the relatively
563 unradiogenic ε_{Nd} values during MIS M2 point to more limited glaciation of North
564 American and Greenland (Lang et al., 2016; this study; Fig. 3g-i; Tab. 1). The second
565 mechanism for large radiogenic ε_{Nd} excursions involves relabelling of NCW via
566 partial dissolution of east Greenlandic- and Icelandic-sourced radiogenic volcanic
567 phases deposited in the Iceland basin, following a shift in the location of the main site
568 of NCW formation from the sea ice-covered Nordic Seas to south of Iceland, and a
569 reduction in unradiogenic Labrador Seawater production (Du et al., 2020). In this
570 case, our data for MIS 2 and MIS 100 signal a slowdown in AMOC (reduced bottom
571 current speeds in the Iceland Basin promotes labelling via partial dissolution of
572 volcanic phases because the longer benthic exposure time that results allows seawater
573 and authigenic ε_{Nd} in this region to converge toward detrital sediment ε_{Nd} (Du et al.,
574 2020)), whereas the muted IG-G shift in ε_{Nd} at Site U1313 during MIS M2 (Tab. 1)

575 signals vigorous formation of NCW in largely ice-free Nordic and Labrador seas.
576 Either way, if radiogenic excursions in the deep North Atlantic during glacials reflect
577 end-member changes in NCW ε_{Nd}, the lack of a large negative excursion in Site
578 U1313 benthic $\delta^{13}C$ during MIS M2 (compare data in red in Fig. 3l and 3g-h; Tab. 1)
579 implies reduced remineralisation of ^{12}C in the deep North Atlantic relative to the Last
580 Glacial Maximum and MIS 100 under a more vigorous AMOC (Pöppelmeier et al.,
581 2020). Thus, regardless as to whether our North Atlantic ε_{Nd} records reflect changes in
582 water-mass provenance or a change in the preformed composition of NCW, they
583 strongly suggest that Atlantic Ocean circulation during MIS M2 was markedly
584 different to that of large Quaternary glaciations with markedly weaker chemical
585 stratification.
586
587 **3.4 Implications for glacial CO_2-storage in the ocean abyss**
588 A ~110 ppm decline in atmospheric CO_2 during MIS M2 (Fig. 6a) strongly implies
589 increased carbon storage in the abyssal ocean (de la Vega et al., 2020). A Southern
590 Ocean-focused driving mechanism is favoured by de la Vega et al. (2020) because the
591 tail end of the CO_2 decline documented appears out of phase with the decline in
592 northern hemisphere insolation and benthic $\delta^{18}O$ but in-phase with both insolation
593 decline at 65°S (compare CO_2 record in Fig. 6a to data in black in 6b,f) and Nd
594 isotope-based evidence for SCW incursion into the North Atlantic (Lang et al. (2016)
595 (compare Fig. 6a to U1313 ε_{Nd} data points denoted by grey boxes in 6c). Yet, in
596 contrast to previous suggestions (e.g., Lang et al., 2016), we find that SCW expansion
597 during MIS M2 was limited to the deep South Atlantic (as tracked by 1267). Our data
598 also suggest that this modest SCW expansion in the Atlantic during MIS M2 peaked
599 ~10-15-kyr before minimum values in atmospheric CO_2 were reached during this

glacial (compare red horizontal bar in Fig. 6d to CO_2 data in 6a). Together, these observations imply that the deep Atlantic was not the ultimate store for the CO_2 sequestered from the atmosphere during this cold stage. Future work should focus on the possibility that the deep Pacific played a major CO_2 storage role, as hinted at by the temporal relationship between benthic $\delta^{13}C$ at Site 1123 and atmospheric CO_2 during MIS M2 (compare Fig. 6a to 1123 $\delta^{13}C$ data in blue in 6d).

3.5 How sluggish was AMOC during MIS M2?

The lag between atmospheric CO_2 and benthic $\delta^{18}O$ during MIS M2 (Section 3.4) implies that high latitude cooling and glaciation during this cold stage were not simply controlled by radiative forcing from greenhouse gases. Instead, other mechanisms must have been important. One mechanism invoked to have played at least a part in amplifying glaciation of the high northern latitudes is AMOC weakening (De Schepper et al., 2013).

AMOC suppression of a magnitude comparable to that reconstructed for major Quaternary glaciations including the Last Glacial Maximum (e.g., Naafs et al., 2010; Bolton et al., 2018), is invoked for M2 based on evidence from dinoflagellate assemblages for a southward deflection of the North Atlantic Current (NAC) to ~41˚N (see panel '3' in Figure 6 of De Schepper et al., 2013) and significant reductions in North Atlantic SSTs (of up to 6˚C; Fig. 7f). The sediment abundance of the dinoflagellate *Operculodinium centrocarpum*, which has a strong affinity with NAC waters in the modern (De Schepper et al., 2013), in Site U1308 (50˚N) and 610 (53˚N) (Fig. 7g) provide evidence for NAC weakening and/or its deflection south of ~50˚N throughout MIS M2 (Fig 8c). The abundance of *O. centrocarpum* in Site U1313 sediments deposited at 41˚N during this cold stage is only high, however, during early

625 glacial conditions (Fig. 7h), indicating that maximum southward deflection of the
626 NAC during this time occurred well before the full glacial MIS M2 (Fig. 8d). An
627 early glacial timing for maximum NAC decline during MIS M2 is consistent with our
628 observation that SCW incursion into the deep Atlantic reached its MIS M2 peak
629 before ~3295 ka (compare Fig. 7b-c to 7h).

630 Palaeoceanographic records suggest that AMOC can remain relatively strong in
631 the face of a significant reduction in the volumetric extent of NCW (e.g., Böhm et al.,
632 2015). Yet, numerical models of ocean circulation indicate that if AMOC vigour
633 during MIS M2 was comparable to the Last Glacial Maximum, it should be associated
634 with a similarly large (i.e., late Pleistocene glacial-like) reduction in the volumetric
635 importance of the NCW overturning cell (e.g., Nikurashin and Vallis, 2011; Kostov et
636 al., 2014; Burke et al., 2015). If changes in ε_{Nd} at U1313 reflect the magnitude of
637 SCW incursion into the deep North Atlantic during our three target glacials, our new
638 datasets show that M2 was not associated with NCW shoaling on the scale of the last
639 glacial or even MIS 100, 2.52 Ma (Fig. 4d-f, j-l). If the evolution of ε_{Nd} at U1313
640 instead reflects changes in the preformed composition of NCW (e.g., Zhao et al.,
641 2019; Pöppelmeier et al., 2020), the small amplitude of IG-G change in ε_{Nd} and
642 benthic $\delta^{13}C$ at this site during MIS M2 would also be inconsistent with a
643 significantly weaker-than-modern AMOC (see Section 3.3.1). Either way, our new
644 records strongly suggest that AMOC during this cold stage was not as sluggish as
645 during major Quaternary glacials.

646 Our interpretations are consistent with the surface temperature history of the
647 North Atlantic. A ~6˚C decline in SSTs in the subpolar North Atlantic during MIS
648 M2 provides clear evidence for a reduction in northward heat transport from a
649 warmer-than-pre-industrial baseline but temperatures remained as warm (Sites 982

and U1313) or warmer (Sites 642 and 610) than the Holocene average (Fig. 7f). These observations may help us to understand why firm evidence for glacial expansion in the high northern latitudes ~3.3 Ma is limited to circum-Arctic landmasses, Greenland, Svalbard and Iceland (De Schepper et al., 2014; Tan et al., 2017). We note that sediments interpreted as glacial tills from mid-latitude James Bay Lowland, Canada, have been loosely dated to ~3.5 Ma (Gao et al., 2012), but this interpretation has been called into question (Clague et al., 2020).

4. Conclusions

We present new Nd isotope data and benthic foraminiferal B/Ca ratios for southeast Atlantic Site 1267 (29˚S, ~4350 m water depth) and northwest Atlantic Site U1313 (41˚N, ~3400 m water depth) spanning the last glacial-Holocene, MIS 100, 2.52 Ma, and MIS M2, ~3.3 Ma, often inferred to signal a prelude to Quaternary extensive glaciation of the northern hemisphere and therefore a bi-polar Cenozoic icehouse climate state. We demonstrate that Southern Component Water expanded into the deep South and North Atlantic during MIS 100. The resulting glacial water-mass properties at our study sites are comparable to those that we document for the last glacial. This Quaternary glacial picture contrasts with the one that we document for MIS M2, in which Northern Component Water persists in the deep North Atlantic.

Our new observations are incompatible with AMOC suppression during MIS M2 to the scale of MIS 100 or 2 and suggest that the atmospheric CO_2 decline during this cold stage was not achieved by carbon storage in the deep Atlantic Ocean, implying storage in deep Pacific Ocean reservoirs. Our findings, together with Holocene-like surface ocean temperatures in the high latitude North Atlantic, help to resolve the mystery of why there is no evidence to suggest that the

675 northern hemisphere was extensively glaciated during M2.

676

677 **5. Acknowledgements**

678 This research uses samples provided by the IODP, which is sponsored by the U.S.
679 National Science Foundation and participating countries under management of Joint
680 Oceanographic Institutions, Inc. We thank the shipboard party of IODP Expedition
681 306 and A. Wuelbers and W. Hale for their help at the Bremen Core Repository and
682 Bastian Hambach and Megan Spencer for laboratory support in Southampton. We
683 also thank the editor Antje Voelker and three anonymous reviewers for comments and
684 suggestions that helped to improve this manuscript considerably. I.B. acknowledges
685 support from the EU project MARINEFF (Interreg VA France-(Channel)-England
686 Programme project #162). M.E.R. acknowledges support from the Vetlesen
687 Foundation. P.A.W. and G.L.F. acknowledge funding from Royal Society Wolfson
688 Merit Awards and NERC grants NE/F00141X/1 to P.A.W. and I.B. and NE/T012382
689 to P.A.W. and A.B.

690

691 **Data Availability:** The data presented in this manuscript will be made available upon
692 request. These data will be deposited in PANGAEA upon acceptance on this
693 manuscript for publication.

694

695 **Declaration of interests:** none.

696

697 **Author Contributions:** N.K generated the Site 1267 data and contributed to
698 manuscript writing; I.B. designed the study, supervised N.K. in data generation and
699 wrote the manuscript; A.B generated the Site U1313 stable isotope data for MIS 100

and contributed to manuscript writing; T.B.C. supervised R.L.P in generating the Site 1267 benthic B/Ca data and contributed to the ideas presented and to manuscript writing; R.L.P generated a subset of the Site 1267 data; A.J.C. supervised N.K. and R.L.P in data generation, contributed to the ideas presented and to manuscript writing; V.E.T. supervised N.K. and R.L.P. in data generation, generated the volcanic glass count data and contributed to manuscript writing; J.A.M helped to generate the Nd isotope data; G.L.F. contributed to the ideas presented and manuscript writing; M.E.R. contributed to the ideas presented and manuscript writing; D.K. contributed samples and to the ideas presented and manuscript writing; D.B.B contributed samples and to manuscript writing; P.A.W. designed the study, supervised N.K. in data generation, co-wrote the manuscript with I.B.

6. References

Arhan, M., Mercier, H., Park, Y.-H., 2003. On the deep water circulation of the eastern South Atlantic Ocean. Deep-Sea Research I 50, 889-916. doi:10.1016/S0967-0637(03)00072-4

Bachem, P.E., Risebrobakken, B., De Schepper, S., McClymont, E.L., 2017. Highly variable Pliocene sea surface conditions in the Norwegian Sea. Climate of the Past 13 1153-1168, doi:10.5194/cp- 13-1153-2017

Bayon, G., German, C.R., Boella, R.M., Milton, J.A., Taylor, R.N., Nesbitt, R.W., 2002. An improved method for extracting marine sediment fractions and its application to Sr and Nd isotopic analysis. Chemical Geology187, 179–199.

Bayon, G., German, C.R., Nesbitt, R.W., Bertrand, P., Schneider, R.R., 2003. Increased input of circumpolar deep water-borne detritus to the glacial SE

725 Atlantic Ocean, Geochem. Geophys. Geosyst. 4(3), 1025,
726 doi:10.1029/2002GC000371.
727 Bayon, G., Burton, J.W., Soulet, G., Vigier, N., Dennielou, B., Etoubleau, J.,
728 Ponzevera, E., German, C.R., Nesbitt, R.W.,2009. Hf and Nd isotopes in
729 marine sediments: Constraints on global silicate weathering. EPSL 277, 318–
730 326. doi:10.1016/j.epsl.2008.10.028.
731 Bell, D.B., Jung, S.J.A., Kroon, D., Lourens, L.J., Hodell, D.A., 2014. Local and
732 regional trends in Plio-Pleistocene d^{18}O records from benthic foraminifera.
733 Geochem. Geophys. Geosystems. http://dx.doi.org/10.1002/2014GC005297.
734 Bell, D.B., Jung, S.J.A., Kroon, D., 2015. The Plio-Pleistocene development of
735 Atlantic deep-water circulation and its influence on climate trends. Quaternary
736 Science Reviews 123, 265-282.
737 http://dx.doi.org/10.1016/j.quascirev.2015.06.026.
738 Blaser, P., Lippold, J., Gutjahr, M., Frank, N., Link, J.M., Frank, M., 2016. Extracting
739 foraminiferal seawater Nd isotope signatures from bulk deep sea sediment by
740 chemical leaching. Chemical Geology 439, 189-204.
741 http://dx.doi.org/10.1016/j.chemgeo.2016.06.024.
742 Böhm, E. et al., 2015. Strong and deep Atlantic meridional overturning circulation
743 during the Last Glacial Cycle. *Nature* 517, 73–76.
744 Bolton, C.T., Wilson, P.A., Bailey, I., Friedrich, O., Beer, C.J., Becker, J., Baranwal,
745 S., Schiebel, R., 2010. Millennial- scale climate variability in the subpolar
746 North Atlantic Ocean during the late Pliocene, Paleoceanography 25, PA4218,
747 doi:10.1029/2010PA001951.
748 Bolton, C.T., Bailey, I., Friedrich, O., Tachikawa, K., de Garidel-Thoron, T., Vidal,
749 L., et al., 2018. North Atlantic midlatitude surface-circulation changes

through the Plio-Pleistocene intensification of Northern Hemisphere glaciation. Paleoceanography and Paleoclimatology, 33. https://doi.org/10.1029/2018PA003412.

Bond, G.C., Lotti, R., 1995. Iceberg discharges into the North Atlantic on millennial time scales during the last glaciation. Science 267, 1005-1010.

Brigham-Grette, J. et al., 2013. Pliocene warmth, polar amplification, and stepped Pleistocene cooling recorded in NE Arctic Russia. Science 340, 1421–1426.

Burke, A., Stewart, A.L., Adkins, J.F., Ferrari, R., Jansen, M.F., Thompson, A.F., 2015. The glacial mid-depth radiocarbon bulge and its implications for the overturning circulation, Paleoceanography 30, 1021–1039, doi:10.1002/2015PA002778.

Burton, K.W., Ling, H.F., O'Nions, R.K., 1997. Closure of the Central American Isthmus and its effect on deep-water formation in the North Atlantic. Nature 386, 382–385. doi:10.1038/386382a0.

Burton, K.W., Lee, D.-C., Christensen, J.N., Halliday, A.N., Hein, J.R., 1999. Actual timing of neodymium isotope variations recorded by FeMn crusts in the western North Atlantic. EPSL 171, 149–156. doi:10.1016/S0012-812X(99)00138-7.

Cande, S.C., Kent, D.V., 1995. Revised calibration of the geomagnetic polarity timescale for the Late Cretaceous and Cenozoic. J. Geophys. Res. 1000 (B4), 6093–6095.

Chalk, T.B., Foster, G.L., Wilson, P.A., 2019. Dynamic storage of glacial CO_2 in the Atlantic Ocean revealed by boron [CO_3^{2-}] and pH records. EPSL 510, 1–11.

Choboter, P.F., Swaters, G.E., 2000. Modelling equator-crossing currents on the ocean bottom. Canadian Applied Mathematics Quarterly 8(4), 367–385.

775 Clague, J.J., Barendregt, R.W., Menounos, B., Roberts, N.J., Rabassa, J., Martinez,
776 O., Ercolano, B., Corbella, H., Hemming, S.R., 2020. Pliocene and Early
777 Pleistocene glaciation and landscape evolution on the Patagonian Steppe,
778 Santa Cruz province, Argentina. Quat. Sci. Revs. 227, 105992.
779 https://doi.org/10.1016/j.quascirev.2019.105992.
780 Coles, V.J., McCartney, M.S., Olson, D.B., Smethie Jr., W.M., 1996. Changes in
781 Antarctic Bottom Water properties in the western South Atlantic in the late
782 1980s. Journal of Geophysical Research 101, C3. 8957–8970.
783 Connary, S.D., Ewing, M., 1974. Penetration of Antarctic Bottom Water from the
784 Cape Basin into the Angola Basin. Journal of Geophysical Research 79, 463–
785 469.
786 Crocker, A.J., Chalk, T.B., Bailey, I., Spencer, M.R., Gutjahr, M., Foster, G.L.,
787 Wilson, P.A., 2016. Geochemical response of the mid-depth Northeast
788 Atlantic Ocean to freshwater input during Heinrich events 1 to 4. Quaternary
789 Science Reviews 151, 236-254.
790 DeConto, R.M., Pollard, D., Wilson, P.A., Palike, H., Lear, C.H., Pagani, M., 2008.
791 Thresholds for Cenozoic bipolar glaciation. Nature 455, 652–656. http://
792 dx.doi.org/10.1038/nature07337.
793 Demidov, A.N., Morozov, E.G., Neiman, V.G., 2006. Structure and variability of
794 deep waters in the Romanche Fracture Zone Dokl. Earth Sc. 410: 1136.
795 https://doi.org/10.1134/S1028334X06070300.
796 DePaolo, D., Wasserburg, G., 1976. Nd isotopic variations and petrogenetic models.
797 Geophysical Research Letters 3, 249–252. 10.1029/GL003i005p00249.
798 de la Vega, E., Chalk, T.B., Wilson, P.A., Bysani, R.P., Foster, G.L.,2020.
799 Atmospheric CO_2 during the Mid-Piacenzian Warm Period and the M2

glaciation. Scientific Reports 10, 11002. https:// doi.org/10.1038/s41598-020-67154-8.

De Schepper, S., Head, M.J., Groeneveld, J., 2009. North Atlantic Current variability through marine isotope stage M2 (circa 3.3 Ma) during the mid-Pliocene, Paleoceanography 24, PA4206. doi:10.1029/2008PA001725.

De Schepper, S., Groeneveld, J., Naafs, B.D.A., Van Renterghem, C., Hennissen, J., et al., 2013. Northern Hemisphere Glaciation during the Globally Warm Early Late Pliocene. PLoS ONE 8(12): 81508. doi:10.1371/journal.pone.0081508

De Schepper, S., Gibbard, P.L., Salzmann, U., Ehlers, J., 2014. A global synthesis of the marine and terrestrial evidence for glaciation during the Pliocene Epoch. Earth-Science Reviews 135. doi:10.1016/j.earscirev.2014.04.003.

Dolan, A.M., Haywood, A.M., Hunter, S.J., Tindall, J.C., Dowsett, H.J., Hill, D.J., Pickering, S.J., 2015. Modelling the enigmatic Late Pliocene Glacial Event – Marine Isotope Stage M2, Global and Planetary Change 128, 47–60, http://dx/doi.org/10.1016/j.gloplacha.2015.02.001.

Dowsett, H.J., Robinson, M.M., Haywood, A.M., Hill, D.J., Dolan, A.M., Stoll, D.K., Chan, W.-L., Abe-Ouchi, A., Chandler, M.A., Rosenbloom, N.A., Otto-Bliesner, B.L., Bragg, F.J., Lunt, D.J., Foley, K.M., Riesselman, C.R, 2012. An assessment of confidence in Pliocene global sea-surface temperature, Nature Clim. Change 2, 365-371, doi:10.1038/nclimate1455.

Du, J., Haley, B.A., Mix, A.C., 2020. Evolution of the Global Overturning Circulation since the Last Glacial Maximum based on marine authigenic neodymium isotopes. QSR 241, 106396. https://doi.org/10.1016/j.quascirev.2020.106396.

Dwyer, G.S., Chandler, M.A., 2009. Mid- Pliocene sea level and continental ice volume based on coupled benthic Mg/Ca palaeotemperatures and oxygen

825 isotopes, Philos. Trans. R. Soc. Ser. A, 367, 157–168, doi:10.1098/
826 rsta.2008.0222.
827 Expedition 306 Scientists, 2006. Site U1313. In: North Atlantic Climate, Proceedings
828 of the Integrated Ocean Drilling Program, 303/306,
829 http://dx.doi.org/10.2204/iodp.%20proc.303306.112.2006.
830 Farmer, J.R. et al., 2019. Deep Atlantic Ocean carbon storage and the rise of 100,000-
831 year glacial cycles. Nature Geosciences 12, 355-360.
832 https://doi.org/10.1038/s41561-019-0334-6.
833 Foster, G.L., Vance, D., Prytulak J., 2007. No change in the neodymium isotope
834 composition of deep water exported from the North Atlantic on glacial-
835 interglacial time scales. Geology 35(1). 37–40. doi:10.1130/G23204A.1.
836 Frank, M., Whiteley, N., Kasten, S., Hein, J.R., O'Nions, K., 2002. North Atlantic
837 deep water export to the Southern Ocean over the past 14 Myr: Evidence from
838 Nd and Pb isotopes in ferromanganese crusts. Paleoceanography 17, 12-11-12-
839 19. doi:10.1029/2000pa000606.
840 Gao, C., McAndrews, J.H., Wang, X., Menzies, J., Turton, C.L., Wood, B.D., Pei, J.,
841 Kodors, C., 2012. Glaciation of North America in the James Bay Lowland,
842 Canada, 3.5 Ma, Geology 40(11), 975–978, doi:10.1130/G33092.1
843 Garzoli, S.L., Dong, S., Fine, R., Meinen, C.S., Perez, R.C., Schmid, C., von Sebille,
844 E., Yao, Q., 2015. The fate of the Deep Western Boundary Current in the South
845 Atlantic. Deep-Sea Research I 103, 125–136.
846 Gu, S., Liu, Z., Jahn, A., Rempfer, J., Zhang, J., Joos, F., 2019. Modelling
847 neodymium isotopes in the ocean component of the Community Earth System
848 Model (CESM1). Journal of Advances in Modeling Earth Systems 11(3) 624-
849 640. Doi:10.1029/2018MS001538.

Haug, G.H., Tiedemann, R., 1998. Effect of the formation of the Isthmus of Panama on Atlantic Ocean thermohaline circulation, Nature 393, 673–676.

Haywood, A.M., et al., 2013. On the identification of a Pliocene time slice for data-model comparison. Philos. Trans. A Math. Phys. Eng. Sci. 371(2001): 20120515. doi:10.1098/rsta/2012.0515.

Hillaire-Marcel, C., de Vernal, A., Bilodeau, G., Weaver, A.J., 2001a. Absence of deep-water formation in the Labrador Sea during the last interglacial period. Nature 410, 1073–1077. https://doi.org/10.1038/35074059.

Hillaire-Marcel, C., de Vernal, A., Candon, L., Bilodeau, G., Stoner, J., 2001b. Changes of Potential Density Gradients in the Northwestern North Atlantic During the Last Climatic Cycle Based on a Multiproxy Approach. in The Oceans and Rapid Climate Change: Past, Present, and Future. Geophys. Monogr., 126, edited by D. Seidov, B. J. Haupt, and M. Maslin, pp. 83–100, AGU, Washington, D. C. https://doi.org/10.1029/GM126p0083.

Hodell, D.A., Venz, K.A., 1992. Toward a high-resolution stable isotopic record of the Southern Ocean during the Pliocene-Pleistocene (4.8 to 0.8 Ma), Antarctic Research Series 56, 265–310.

Hodell, D.A., Venz-Curtis, K.A., 2006. Late Neogene history of deepwater ventilation in the Southern Ocean. Geochem. Geophys. Geosyste. 7, Q09001.

Howe, J.N.W., Piotrowski, A.M., Noble, T.L., Mulitza, S., Chiessi, C.M., Bayon, G., 2016. North Atlantic Deep Water Production during the Last Glacial Maximum. Nature Communications 7, 11765. doi:10.1038/ncoms11765.

Hu, R., Noble, T.L., Piotrowski, A.M., McCave, I.N., Bostock, H.C., Neil, H.L., 2016. Neodymium isotopic evidence for linked changes in Southeast Atlantic

874 and Southwest Pacific circulation over the last 200 kyr. Earth Planet. Sci. Lett.
875 455, 106–114. https://doi.org/10.1016/j.epsl.2016.09.027.
876 Huang, H., Gutjahr, M., Eisenhauer, A., and Kuhn, G., 2020. No detectable Weddell
877 Sea Antarctic Bottom Water export during the Last and Penultimate Glacial
878 Maximum: Nature Communications 11, 424, https://doi.org/10.1038/ s41467-
879 020-14302-3.
880 Jansen, E., Fronval, T., Rack, F., Channell, J.E.T., 2000. Pliocene-Pleistocene ice
881 rafting history and cyclicity in the Nordic Seas during the last 3.5 Myr,
882 Paleoceanography 15(6), 709–721.
883 Jeandel, C., 1993. Concentration and isotopic composition of Nd in the South Atlantic
884 Ocean. EPSL 117(3–4), 581–591. https://doi.org/10.1016/0012-821(93)90104-
885 H.
886 Keigwin, L.D., 1987. Pliocene stable-isotope record of Deep Sea Drilling Project Site
887 606: Sequential events of ^{18}O enrichment beginning at 3.1 Ma, Initial Rep.
888 Deep Sea Drill. Proj., 94, 911–920.
889 Kerr, J., Rickaby, R., Yu, J., Elderfield, H., Sadekov, A.Y., 2017. The effect of ocean
890 alkalinity and carbon transfer on deep-sea carbonate ion concentration during
891 the past five glacial cycles. EPSL 471, 42–53.
892 Kostov, Y., Armour, K.C., Marshall, J., 2014. Impact of the Atlantic meridional
893 overturning circulation on ocean heat storage and transient climate change.
894 Geophys. Res. Lett., 41(6), 2108–2116.
895 Lambeck, K., Rouby, H., Purcell, A., Sun, Y., Sambridge, M., 2014. Sea level and
896 global ice volumes from the Last Glacial Maximum to the Holocene. PNAS
897 111 (43) 15296-15303. https://doi.org/10.1073/pnas.1411762111.
898 Lambelet, M., van de Flierdt, T., Crocket, K., Rehkämper, M., Kreissig, K., Coles, B.,

899 Rijkenberg, M.J.A., Gerringa, L.J.A., de Baar, H.J.W., Steinfeldt, R., 2016.
900 Neodymium isotopic composition and concentration in the western North
901 Atlantic Ocean: results from the GEOTRACES GA02 section. Geochim.
902 Cosmochim. Acta 177, 1–29. http://dx. doi.org/10.1016/j.gca.2015.12.019.
903 Lang, D.C., Bailey, I., Wilson, P.A., Chalk, T.B., Foster, G.L., Gutjahr, M., 2016.
904 Incursions of southern-sourced water into the deep North Atlantic during late
905 Pliocene glacial intensification. Nature Geoscience volume 9, 375–379.
906 https://doi.org/10.1038/ngeo2688.
907 Lang, D.C., Bailey, I., Wilson, P.A., Beer, C., Bolton, C.T., Newsam, C.,
908 Spencer, M.R., Friedrich, O., Gutjahr, M., Foster, G.L., Cooper, C.J., Milton,
909 A., 2014. The transition on North America from the warm humid Pliocene to the
910 glaciated Quaternary traced by eolian dust deposition at a benchmark North
911 Atlantic Ocean drill site, Quaternary Science Reviews 93C, 125–141.
912 doi:10.1016/j.quascirev.2014.04.005.
913 Laskar, J. et al., 2004. A long-term numerical solution for the insolation quantities
914 of the Earth. A & A, 428. 261–285
915 Lauvset, S.K., Key, R.M., Olsen, A., van Heuven, S., Velo, A., Lin, X., Schirnick, C.,
916 Kozyr, A., Tanhua, T., Hoppema, M., 2016. A new global interior ocean
917 mapped climatology: the 1°× 1° GLODAP version 2. Earth System Science
918 Data Discussions 8, 325–340.
919 Lawrence, K.T., Herbert, T.D., Brown, C.M., Raymo, M.E., and Haywood, A.M.,
920 2009. High-amplitude variations in North Atlantic sea surface temperature
921 during the early Pliocene warm Period, Paleoceanography 24, PA2218,
922 doi:10.1029/2008PA001669.
923 Lippold, J., Gutjahr, M., Blaser, P., Christner, E., de Carvalho Ferreira,. M.L.,

924 Mulitza, S., Christl, M., Frank Wombacher, F., Böhm, E., Antz, B.,
925 Cartapanis, O., Vogel, H., Jaccard, S.L., 2016. Deep water provenance and
926 dynamics of the (de)glacial Atlantic meridional overturning circulation. EPSL
927 445. 68–78. http://dx.doi.org/10.1016/j.epsl.2016.04.013.
928 Lisiecki, L.E., Raymo, M.E., 2005. A Pliocene–Pleistocene stack of 57 globally
929 distributed benthic delta-^{18}O records. Paleoceanography 20, PA1003,
930 http://dx.doi.org/10.1029/2005PA001164.
931 MacLeod, K.G., Martin, E.E., Blair, S.W., 2008. Nd isotopic excursion across
932 Cretaceous ocean anoxic event 2 (Cenomanian-Turonian) in the tropical North
933 Atlantic. Geology 36, 811–814. doi:10.1130/G24999a.1
934 Martin, E.E., Blair, S.W., Kamenov, G.D., Scher, H.D., Bourbon, E., Basak, C.,
935 Newkirk, D.N., 2010. Extraction of Nd isotopes from bulk deep sea sediments
936 for paleoceanographic studies on Cenozoic time scales. Chem. Geol. 269, 414-
937 431.
938 Martin, E.E., Scher, H.D., 2004. Preservation of seawater Sr and Nd isotopes in fossil
939 fish teeth: bad news and good news. Earth Planet. Sci. Lett. 220, 25–39.
940 Martínez-Botí, M.A., Foster, G.L, Chalk, T.B., Rohling, E.J., Sexton, P.F., Lunt, D.J.,
941 Pancost, R.D., Badger, M.P.S., Schmidt, D.N., 2015. Plio-Pleistocene climate
942 sensitivity evaluated using high-resolution CO2 records. Nature 518, 49–54.
943 http:// dx.doi.org/10.1038/nature14145.
944 Maslin, M.A., Li, X. S., Loutre, M.–F., Berger, A., 1998. The contribution of orbital
945 forcing to the progressive intensification of northern hemisphere glaciation,
946 Quat. Sci. Rev., 17, 411–426.
947 McCartney, M.S., Bennett, S.L., Woodgate-Jones, M.E., 1991. Eastward Flow
948 through the Mid-Atlantic Ridge at 11˚N and Its Influence on the Abyss of the

949 Eastern Basin. Journal of Physical Oceanography 21, 1089–1121.
950 McCartney, M.S., 1992. Recirculating components to the deep boundary current of
951 the northern North Atlantic. Prog. Oceanog. 29, 283–383.
952 McClymont, E.L., Ford, H.L., Ho, S.L., Tindall, J.C., Haywood, A.M., Alonso-
953 Garcia, M., Bailey, I., Berke, M.A., Littler, K., Patterson, M.O., Petrick, B.,
954 Peterse, F., Ravelo, A.C., Risebrobakken, B., De Schepper, S., Swann, G.E.A.,
955 Thirumalai, K., Tierney, J.E., van der Weijst, C., White, S., Abe-Ouchi, A.,
956 Baatsen, M.L.J., Brady, E.C., Chan, W.-L., Chandan, D., Feng, R., Guo, C.,
957 von der Heydt, A.S., Hunter, S., Li, X., Lohmann, G., Nisancioglu, K.H.,
958 Otto-Bliesner, B.L., Peltier, W.R., Stepanek, C., Zhang, Z., 2020. Lessons
959 from a high-CO_2 world: an ocean view from ~ 3 million years ago. Clim. Past
960 16, 1599–1615. https://doi.org/10.5194/cp-16-1599-2020.
961 McDonagh, E.L., Arhan, M., Heywood, K.J., 2002. On the circulation of bottom
962 water in the region of the Vema Channel. Deep-Sea Research I 49, 1119–
963 1139.
964 McKay, R., et al., 2012. Antarctic and Southern Ocean influences on Late Pliocene
965 global cooling. PNAS 109(17), 6423–6428. doi:10.1073/PNAS/1112248109.
966 Mercier, H., Morin, P., 1997. Hydrography of the Romanche and Chain Fracture
967 Zones. Journal of Geophysical Research 102(C5), 10373–10389.
968 Mercier, H., Weatherly, G.L., Arhan, M., 2000. Bottom water throughflows at the rio
969 de Janeiro and Rio Grande Fracture Zones. GRL 27(10), 1503–1506.
970 Meredith, M.P., Jullion, L., Brown, P.J., Naveira Garabato, A.C., Couldrey, M.P.,
971 2014. Dense waters of the Weddell and Scotia Seas: recent changes in
972 propertiesand circulation. Philosophical Transactions of the Royal Society A
973 372 (2019) https://doi.org/10.1098/rsta.2013.0041.

974 Miller, K.G., Wright, J.D., Browning, J.V., Kulpecz, A.A., Kominz, M.A.,
975 Naish, T.R., Cramer, B.S., Rosenthal, Y., Peltier, R.W., Sosdian, S., 2012. The
976 high tide of the warm Pliocene: Implications of global sea level for Antarctic
977 deglaciation, Geology, 40, 407–410.
978 Mix, A.C., Pisias, N. G., Rugh, W., Wilson, J., Morey, A., Hagelberg, T.K., 1995.
979 Benthic foraminfer stable isotope record from Site 849 (0-5 Ma): local and
980 global climate changes. *Procs*. *Ocean Drill*. *Prog*, *Sci*. *Res*. 138, 371–412.
981 Mudelsee, M., Raymo, M.E., 2005. Slow dynamics of the northern hemisphere
982 glaciation. Paleoceanography 20, PA4022.
983 http://dx.doi.org/10.1029/2005PA001153.
984 Naafs, B.D.A., Ruediger, S.R., Hefter, J., Khelifi, N., De Schepper, S., Haug, G.H.,
985 2010. Late Pliocene changes in the North Atlantic Current, EPSL 298, 434–442.
986 https://doi.org/10.1016/j.epsl.2010.08.023.
987 Naafs, B.D.A., Hefter, J., Stein, R., 2014. Millennial-scale ice rafting events and
988 Hudson Strait Heinrich(-like) Events during the late Pliocene and Pleistocene: a
989 review. QSR 80, 1-28. http://dx.doi.org/10.1016/j.quascirev.2013.08.014.
990 Naafs, B.D.A., Voelker, A.H.L., Karas, C., Andersen, N., Sierro, F.J., 2020. Repeated
991 near-collapse of the Pliocene sea surface temperature gradient in the North
992 Atlantic. Paleoceanography and Paleoclimatology, 35(5),
993 doi:10.1029/2020PA003905.
994 Naish, T., 1997. Constraints on the amplitude of late Pliocene eustatic sea level
995 fluctuations: new evidence from the New Zealand shallow marine sediment
996 record. Geology 25 (12), 1139–1142, http://dx.doi.org/10.1130/0091-
997 7613(1997)025 < 1139:COTAOL > 2.3.CO;2.
998 Naish, et al., 2009. Obliquity-paced Pliocene West Antarctic ice sheet oscillations.

Nature 458, 322–328. https://doi.org/10.1038/nature07867.

Ng, H.C., Robinson, L.F., McManus, J.F., Mohamed, K.J., Jacobel, A.W., Ivanovic, R.F., Gregoire, L.J., Chen, T., 2018. Coherent deglacia changes in western Atlantic Ocean circulation. Nature Communications 9, 2947, https:// doi.org/10.1038/s41467-018-05312-3.

Nikurashin, M., Vallis, G., 2011. A Theory of Deep Stratification and Overturning Circulation in the Ocean, J. Phys. Oceanogr. 41(3), 485–502, doi:10.1175/2010JPO4529.1.

O'Nions, R.K., Frank, M., von Blanckenburg, F., Ling, H.F., 1998. Secular variation of Nd and Pb isotopes in ferromanganese crusts from the Atlantic, Indian and Pacific Oceans. EPSL 155, 15–28. doi:10.1016/S0012-821x(97)00207-0.

Oppo, D.W., Raymo, M.E., Lohmann, G.P., Mix, A.C., Wright, J.D., Prell, W.L., 1995. A $\delta^{13}C$ record of Upper North Atlantic Deep Water during the past 2.6 million years. Paleoceanog. 10(3), 373-394.

Oppo, D.W., Fairbanks, R.G., 1987. Variability in the deep and intermediate water circulation of the Atlantic Ocean: Northern hemisphere modulation of the Southern Ocean, EPS, 86, 1–15.

Patterson, M.O., McKay, R., Naish, T., Bostock, H. C., Dunbar, R., Ohneiser, C., et al., 2018. A southwest Pacific perspective on long-term global trends in Pliocene-Pleistocene stable isotope records. Paleoceanography and Paleoclimatology 33, 825–839. https:// doi.org/10.1029/2017PA003269.

Pena, L.D., Goldstein, S., 2014. Thermohaline circulation crisis and impacts during the mid-Pleistocene transition. Science 345 (6194). Doi:10.1126/science/1249770.

Piotrowski, A.M., Goldstein, S.L., Hemming, S.R., Fairbanks, R.G., 2005. Temporal

relationships of carbon cycling and ocean circulation at glacial boundaries. Science 307, 1933–1938, doi:10.1126/Science.1104883.

Pöppelmeier, F., Gutjahr, M., Blaser, P., Keigwin, L.D., Lippold, J., 2018. Origin of abyssal water mass in the NW Atlantic since the Last Glacial Maximum. Paleoceanogr. Paleoclimatol. 33 (5), 530–543. https://doi.org/10.1029/2017PA003290.

Pöppelmeier, F., Blaser, P., Gutjahr, M., Süfke, F., Thornalley, D.J.R., Grützner, J., Jakob, K.A., Link, J.M., Szidat, S., Lippold, J., 2019a. Influence of ocean circulation and benthic exchange on deep Northwest Atlantic Nd isotope records during the past 30,000 years. Geochem. Geophys. Geosyst. 20, 4457–4469. https://doi.org/ 10.1029/2019GC008271.

Pöppelmeier, F., Gutjahr, M., Blaser, P., Oppo, D.W., Jaccard, S.L., Regelous, M., Huang, K.-F., Süfke, F., Lippold, J., 2019b. Water mass gradients of the mid-depth Southwest Atlantic during the past 25,000 years. EPSL 531, 115963. https://doi.org/10.1016/j.epsl.2019.115963.

Pöppelmeier, F., Gutjahr, M., Blaser, P., Jaccard, S.L., Frank, M., Max, L., Lippold, J., 2020. Northern-sourced water dominated the Atlantic Ocean during the Last Glacial Maximum. Geology 48. https:// doi.org/10.1130/G47628.1.

Prell, W.L., 1984. Covariance patterns of foraminiferal $\delta^{18}O$: An evaluation of Pliocene ice volume changes near 3.2 million years ago, Science, 226, 692–694, doi:10.1126/ science.226.4675.692.

Rae, J.W., Foster, G.L., Schmidt, D.N., Elliott, T., 2011. Boron isotopes and B/Ca in benthic foraminifera: Proxies for the deep ocean carbonate system. Earth and Planetary Science Letters 302, 403-413.

Raymo, M.E., Ruddiman, W.F., Clement, B.M., 1987. Pliocene/Pleistocene

paleoceanography of the North Atlantic at DSDP Site 609. Initial Reports of the Deep Sea Drilling Project, v.94, p. 895-901.

Raymo, M.E., Ruddiman, W.F., Shackleton, N.J., Oppo, D.W., 1990. Evolution of the Atlantic-Pacific $d^{13}C$ gradients over the last 2.5 m.y., EPSL 97, 353–368.

Raymo, M.E., Hodell, D., Jansen, E., 1992. Response of deep ocean circulation to the initiation of northern hemisphere glaciation (3-2 M.Y.), Paleoceanography, 7, 645–672.

Raymo, M.E., Oppo, D.W., Flower, B.P., Hodell, D.A., McManus, J.F., Venz, K.A., Kleiven, K.F., McIntyre, K., 2004. Stability of North Atlantic water masses in face of pronounced climate variability during the Pleistocene. Paleoceanography 19(2), PA2008, doi:10.1029/2003PA000921.

Reynolds, B., Frank, M., O'Nions, R., 1999. Nd-and Pb-isotope time series from Atlantic ferromanganese crusts: implications for changes in provenance and paleocirculation over the last 8 Myr. *Earth and Planetary Science Letters* **173**, 381-396, doi:10.1016/S0012-821X(99)00243-5.

Reynolds, B.C., Sherlock, S.C., Kelley, S.P., Burton, K.W., 2004. Radiogenic isotope records of Quaternary glaciations: Changes in the erosional source and weathering processes. Geology 32(10), 861-864. Doi:10.1130/G20734.1.

Roberts, N.L., Piotrowski, A.M., 2015. Radiogenic Nd isotope labeling of the northern NE Atlantic during MIS 2. Earth and Planetary Science Letters 423, 125–133. https://doi.org/10.1016/j.epsl.2015.05.011.

Ruddiman, W.F., M.E. Raymo, D.G. Martinson, B.M. Clement, and J. Backman, 1989, Mid-Pleistocene evolution of Northern Hemisphere climate. Paleoceanography 4, 353-412.

Sandoval, F.J., Weatherly, G.L., 2000. Evolution of the Deep Western Current of

1074 Antarctic Bottom Water in the Brazil Basin. Journal of Physical
1075 Oceanography 31, 1140–1460.
1076 Sarnthein, M., Winn, K., Jung, S.J.A., Duplessy, J.-C., Labeyrie, L., Erlenkeuser, H.,
1077 Ganssen, G., 1994. Changes in East Atlantic deepwater circulation over the
1078 last 30,000 years: eight time slice reconstructions. Paleoceanography 9, 209–
1079 267. https://doi.org/10.1029/93PA03301.
1080 Schlitzer, R., 2002. Interactive analysis and visualization of geoscience data with
1081 Ocean Data View. *Computers & Geosciences* 28, 1211–1218,
1082 doi:10.1016/S0098-3004(02)00040-7.
1083 Seki, O., Foster, G.L., Schmidt, D.N., Mackensen, A., Kawamura, K., Pancost, R.D.,
1084 2010. Alkenone and boron-based Pliocene pCO2 records, Earth Planet. Sci.
1085 Lett. 292, 201–211. https://doi.org/10.1016/j.epsl.2010.01.037.
1086 Shackleton, N.J., Hall, M.A., Vincent, E., 2000. Phase relationships between
1087 millennial-scale events 64,000-24,000 years ago. Paleoceanography 15(6), 565–
1088 569. https://doi.org/10.1029/2000PA000513.
1089 Smyth-Wright, D., Boswell, S., 1998. Abyssal circulation in the Argentine Basin.
1090 Journal of Geophysical Research 103(C8), 15845–15851.
1091 Stephens, J.C., Marshall, D.P., 2000. Dynamical Pathways of Antarctic Bottom Water
1092 in the Atlantic. Journal of physical Oceanography 30, 622–640.
1093 Stichel, T., Frank, M., Rickli, J., Haley, B.A., 2012. The hafnium and neodymium
1094 isotope composition of seawater in the Atlantic sector of the Southern Ocean.
1095 Earth Planet. Sci. Lett. 317, 282–294.
1096 Stramma, L., England, M., 1999. On the water masses and mean circulation of the
1097 South Atlantic Ocean. Journal of Geophysical Research 104, C9, 20863–20883.
1098 Tan, N., Ramstein, G., Dumas, C., Contoux, C., Ladant, J.-B., Sepulchre, P., Zhang,

Z., De Schepper, S., 2017. Exploring the MIS M2 glaciation occurring during a warm and high atmospheric CO2 Pliocene background climate. Earth and Planetary Science Letters 472, 266–276.

Tanaka, T., Togashi, S., Kamioka, H., Amakawa, H., Kagami, H., Hamamoto, T., Yuhara, M., Orihashi, Y., Yoneda, S., Shimizu, H., Kunimaru, T., Takahashi, K., Yanagi, T., Nakano, T., Fujimaki, H., Shinjo, R., Asahara, Y., Tanimizu, M., Dragusanu, C., 2000. JNdi-1: a neodymium isotopic reference in consistency with LaJolla neodymium. Chemical Geology 168, 279–281. doi:10.1016/S0009-2541(00)00198-4.

Vance, D., Burton, K., 1999. Neodymium isotopes in planktonic foraminifera: a record of the response of continental weathering and ocean circulation rates to climate change. EPSL 173, 365-379.

Vance, D., Thirlwall, M., 2002. An assessment of mass discrimination in MC-ICPMS using Nd isotopes. Chemical Geology 185, 227-240. 10.1016/S0009-2541(01)00402-8.

Venz, K.A., Hodell, D.A., Stanton, C., Warnke, D.A., 1999. A 1.0 Myr record of glacial North Atlantic intermediate water variability from ODP site 982 in the northeast Atlantic. Paleoceanography 14, 42-52, doi:10.1029/1998pa900013.

Venz, K.A., Hodell, D.A., 2002. New evidence for changes in Plio–Pleistocene deep water circulation from Southern Ocean ODP Leg 177 Site 1090. Palaeogeography, Palaeoclimatology, Palaeoecology 182, 197–220, doi:10.1016/S0031-0182(01)00496-5.

Wienders, N., Arhan, M., Mercier, H., 2000. Circulation at the western boundary of the South and Equatorial Atlantic: Exchanges with the ocean interior. Journal of Marine Research 58, 1007–1039.

1124 Wilson, D.J., Crocket, K.C., van de Flierdt, T., Robinson, L.F. & Adkins, J.F., 2014.
1125 Dynamic intermediate ocean circulation in the North Atlantic during Heinrich
1126 Stadial 1: A radiocarbon and neodymium isotope perspective,
1127 Paleoceanography 29, 1072–1093.
1128 Yu, J.M., Elderfield, H., 2007. Benthic foraminiferal B/Ca ratios reflect deep water
1129 carbonate saturation state. Earth and Planetary Science Letters, 73-86.
1130 Yu, J., Elderfield, H., Piotrowski, A.M., 2008. Seawater carbonate ion-delta C-13
1131 systematics and application to glacial-interglacial North Atlantic ocean
1132 circulation. Earth and Planetary Science Letters 271, 209-220.
1133 Yu, J., Anderson, R.F., Jin, Z., Menviel, L., Zhang, F., Ryerson, F.J., Rohling, E.J.,
1134 2014. Deep South Atlantic carbonate chemistry and increased interocean deep
1135 water exchange during last deglaciation. Quat. Sci. Rev. 90, 80–89.
1136 Zhao, N., Oppo, D.W., Huang, K. et al., 2019. Glacial–interglacial Nd isotope
1137 variability of North Atlantic Deep Water modulated by North American ice
1138 sheet. *Nat Commun*. 10, 5773. https://doi.org/10.1038/s41467-019-13707-z.
1139

1140 **Figure Captions**

1141 **Figure 1.** Climate indicators across marine isotope stage (MIS) M2, ~3.3 Ma, and the
1142 Plio-Pleistocene intensification of northern hemisphere glaciation, ~3.5-2.5 Ma
1143 (Mudelsee and Raymo, 2005): **(A)** Site U1313 ε_{Nd} composition of fish debris (Lang et
1144 al., 2016). Estimates of the ε_{Nd} composition of Northern Component Water, NCW,
1145 (red bar) follow Lang et al. (2016) and is taken as the average value of Fe-Mn crust
1146 ε_{Nd} (and their 2 s.d.) from TR079-D14 (Reynolds et al., 1999), BM1969.05 (Burton et
1147 al., 1997; 1999; on chronology of O'Nions et al., 1998), ALV539 2-1 (Burton et al,
1148 1999; on chronology of O'Nions et al., 1998) spanning 2.4-3.3 Ma. Estimate for

Southern Component Water, SCW, (blue bar) is average value of Fe-Mn crust ε_{Nd} (and their 2 s.d.) from D18-1 (Frank et al., 2002) spanning 2.4-3.3 Ma; **(B)** Site U1313 (Lang et al., 2014), Site 1267 (Bell et al., 2014) and ODP Site 982 (Hodell and Venz-Curtis, 2006) benthic $\delta^{13}C$; **(C)** a stack of globally representative benthic $\delta^{18}O$ records, the LR04 (grey; Lisiecki and Raymo, 2005) and benthic $\delta^{18}O$ from North Atlantic Ocean IODP Site U1313 (black; Bolton et al., 2010) and Walvis Ridge (red; Bell et al., 2014). The mid Piacenzian warm period (mPWP) is labelled. The black/white bar at the bottom of the figure denotes palaeomagnetic (sub)chronozones (Cande and Kent, 1995); M = Matuyama, G = Gauss, K = Keana and Ma = Mammoth. See Figure 2 and Supplementary Figure S1 for site locations.

Figure 2. Location of Atlantic Ocean drill sites used in this study (Sites 1267 and U1313, red circles) and others (black circles) discussed in the main text. Also shown is a schematic of modern pathways of deep-waters relevant to our study sites: NADW = North Atlantic Deep Water (dark grey lines), AABW = Antarctic Bottom Water (light blue lines), LSW = Labrador Sea Water, DSOW = Denmark Strait Overflow Water, ISOW = Iceland Scotland Overflow Water (ISOW), WTRO = Wyville Thomson Ridge Overflow, NGS = Norwegian Greenland Seas. The Verma (VFZ), Romanche (RGZ), Chain (CFZ), Rio de Janeiro (RJFZ) and Rio Grande (RGFZ) fracture zones and Walvis Passage (WP) are also labelled and represent important pathways for AABW to the eastern Atlantic (see main text). The Kane Gap (GP) is also labelled. Depths stated for VFZ, RGZ, RJFZ and RGFZ are known maximum depths through which SCW can pass through these fracture zones. Bottom-water pathway reconstructions based on: McCartney et al. (1991); McCartney (1992); Coles et al. (1996); Smyth-Wright and Boswell (1998); Stramma and England (1999);

Wienders et al. (2000); Sandoval and Weatherly (2000); Choboter and Swaters (2000); Mercier et al. (2000); Stephens and Marshall (2000); McDonagh et al. (2002); Arhan et al. (2003); Meredith et al. (2014); Garzoli et al. (2015).

Figure 3. Water-mass provenance tracers from ODP Site 1267 (red) and IODP Site U1313 for the last glacial-Holocene, MIS 100 and MIS M2. (A-C) fresh volcanic glass per gram of dry sediment at Site U1313. Last glacial volcanic glass data in A is from Lang et al. (2016). MIS 100 and MIS M2 volcanic glass data in B and C were generated in this study; (D-F) benthic B/Ca data from Site 1267; (G-I) fish debris Nd isotope data (ε_{Nd}) from sites 1267 and U1313; (J-L) benthic $\delta^{13}C$ and (M-O) benthic $\delta^{18}O$ data from sites 1267 and U1313. Error bars (2 s.d.) for stable isotope data reported by Bolton et al. (2010) for Site U1313 (benthic $\delta^{18}O$ = 0.065‰; benthic $\delta^{13}C$ = 0.031‰), by Bell et al. (2014) for Site 1267 (benthic $\delta^{18}O$ and $\delta^{13}C$ = < 0.1‰) and by Chalk et al. (2019) for Site U1313 (benthic $\delta^{18}O$ = 0.08‰; benthic $\delta^{13}C$ = 0.02‰) are not shown. See Figure 2 for site locations.

Figure 4. Comparison of water-mass provenance tracers predominantly from the Atlantic Ocean for the last glacial-Holocene, MIS 100 and MIS M2: (A-C) [CO_3^{2-}] estimates based on benthic B/Ca data; (D-F) fish debris Nd isotope data (ε_{Nd}) from sites 1267 and U1313 alongside estimates of the ε_{Nd} composition of Northern Component Water (NCW) and the Southern Component Water (SCW) end-members. NCW for MIS M2 and MIS 100 is estimated following Lang et al. (2016) and is taken as the average value of Fe-Mn crust ε_{Nd} (and their 2 s.d.) from TR079-D14 (Reynolds et al., 1999), BM1969.05 (Burton et al., 1997; 1999; on chronology of O'Nions et al., 1998), ALV539 2-1 (Burton et al, 1999; on chronology of O'Nions et al., 1998)

spanning 2.4-3.3 Ma. Also shown in (D) is a composite Nd isotope record from KNR198 from the New England Slope in the northwest North Atlantic, considered by Zhao et al. (2019) to record the evolution of NCW over the past ~21 ka. Estimate for the SCW end-member during MIS M2 and MIS 100 is average value of Fe-Mn crust ε_{Nd} (and their 2 s.d.) from D18-1 (Frank et al., 2002) spanning 2.4-3.3 Ma. Last glacial-Holocene NADW defined as average (and their 2 s.d.) of Holocene U1313 data (<14 ka; MIS 2/1 boundary as defined by Lisiecki and Raymo, 2005). Last glacial-Holocene SCW end-member estimated using an average value of Fe-Mn crust ε_{Nd} (and their 2 s.d.) from D18-1 (Frank et al., 2002) spanning 0-0.04 Ma. Vertical range bars in D show range of modern Upper and Lower North Atlantic Deep Water (UNADW and LNADW, respectively) ε_{Nd} (Lambelet et al., 2016); (G-I) fresh volcanic glass and ice-rafted debris (IRD) >150 μm per gram of dry sediment at Site U1313. Last glacial, MIS 100 and MIS M2 IRD data from Lang et al. (2014), Lang et al. (2016) and Bolton et al. (2010); (J-L) benthic $\delta^{13}C$ data (including estimates of the $\delta^{13}C$ of NCW and SCW); (M-O) benthic $\delta^{18}O$ data. Error bar shown for benthic $\delta^{13}C$ ($\delta^{18}O$) signifies that the uncertainty for the different sources of these data plotted is no larger than 0.1 ‰ (0.15 ‰) at 2 s.d. See Figure 2 and Supplementary Figure S1 for site locations.

Figure 5. $\delta^{13}C$: $[CO_3^{2-}]$ cross plot. B/Ca-derived carbonate data and co-occurring $\delta^{13}C$ data from ODP Site 1267 for Marine Isotope Stage, MIS, 2-Holocene (A), and MIS 99, 100, 101, M1, M2 and MG1 (B). Data from IODP U1313 (hollow green interglacial circles and solid green glacial circles; Chalk et al., 2019), IODP U1308 (hollow black interglacial circles and solid black glacial circles; Chalk et al., 2019), ODP 980 (hollow light brown interglacial circles and solid light brown glacial circles;

Chalk et al., 2019) are also shown in (A). Shown in both panels are shaded endmember compositions for the Southern Ocean (grey oval, Yu et al., 2014) and the Pacific (yellow oval, Kerr et al. (2017), based on Last Glacial Maximum and Holocene data from these regions. The Last Glacial Maximum northern (NADW) endmember is assumed to be denoted by the cluster of glacial ODP 980 points (solid light brown circles). Calculated slopes for CO_2 addition/evasion due to AABW-NADW mixing only (pale blue, dashed) and biological utilization (black, dashed) are shown. Sample gradients for alkalinity and temperature change are also shown, following Yu et al. (2008). See Figure 2 for site locations.

Figure 6. Palaeoceanographic proxies spanning marine isotope stage (MIS) M2, ~3.3 Ma: (A) interpolated 1-kyr resolution $\delta^{11}B$-derived CO_2 data from *Globigerinoides ruber* white *sensu stricto* (with a 6-point running mean) at ODP Site 999 (Martinez-Boti et al., 2015; de la Vega et al., 2020). Shading = 68% (dark red) and 95% (light red) confidence intervals; (B) summer boreal (June 21st) and austral (December 21st) insolation forcing at 65˚N and 65˚S, respectively (Laskar, 2004); (C) Site U1313 benthic $\delta^{13}C$ (Lang et al., 2014) and fish debris ε_{Nd} (thus study; Lang et al., 2016) and estimates of the $\delta^{13}C$ of NCW (Site 982; Venz et al., 1999) and SCW (Site 849; Mix et al., 1995; Site 1123; Patterson et al., 2018) with data symbols removed for clarity; (D) Site 1267 benthic $\delta^{13}C$ (Lang et al., 2014) and fish debris ε_{Nd} (thus study) and estimates of the $\delta^{13}C$ of NCW (Site 982; Venz et al., 1999) and SCW (Site 849; Mix et al., 1995; Site 1123; Patterson et al., 2018) with data symbols removed to aid plotting clarity; (E) [CO_3^{2-}] estimates from Site 1267 based on benthic B/Ca data; (F) Benthic $\delta^{18}O$ data from Site U1313 (Bolton et al., 2010) and Site 1267 (this study). Horizontal dashed line in D represents atmospheric CO_2 value considered to be an

important threshold for extensive glaciation of continents in the northern hemisphere (De Conto et al., 2008). All records plotted on LR04-based age models. See Figure 2 and Supplementary Figure S1 for site locations.

Figure 7. Palaeoceanographic proxies spanning marine isotope stage (MIS) M2, ~3.3 Ma and periods of early and late Pliocene warmth: (A) globally representative benthic $\delta^{18}O$ stack the LR04 (grey; Lisiecki and Raymo, 2005) and benthic $\delta^{18}O$ from North Atlantic Ocean IODP Site U1313 (black; Bolton et al., 2010); (B) fish debris Nd isotope data (ε_{Nd}) from sites 1267 and U1313 alongside estimates of the ε_{Nd} composition of NCW and SCW water-mass end-member (see Figure 4 and main text for methods); (C) benthic $\delta^{13}C$ data from sites 1267 and U1313 and estimates of the $\delta^{13}C$ of Northern component waters (NCW) and southern component waters (SCW); (D) interpolated 1-kyr resolution $\delta^{11}B$-derived CO_2 data from *Globigerinoides ruber* white *sensu stricto* (with a 6-point running mean) at ODP Site 999 (Martinez-Boti et al., 2015; de la Vega et al., 2020). Shading = 68% (dark red) and 95% (light red) confidence intervals; (E) summer boreal (June 21st) and austral (December 21st) insolation forcing at 65˚N and 65˚S, respectively (Laskar, 2004); (F) Alkenone-based reconstructions of sea-surface temperature (SST) from Nordic Seas ODP Hole 642B at 67˚N (Bachem et al., 2017), subpolar North Atlantic subpolar North Atlantic ODP Site 982 at 58˚N (Lawrence et al., 2009), DSDP Hole 610A at 53˚N (Naafs et al., 2020) and IODP Site U1313 at 41˚N (Naafs et al., 2010); abundance of dinoflagellate cyst *Operculodinium centrocarpum* (De Schepper et al., 2009; De Schepper et al., 2013), with increased numbers taken to indicate the presence of the NAC over a study site (De Schepper et al., 2013), at (G) DSDP Site 610 and IODP Site U1308, and at (H) Site U1313 (De Schepper et al., 2013). All data plotted on LR04 or respective published age models.

mPWP = mid Piacenzian Warm Period. Horizontal dashed line in D represents atmospheric CO_2 value considered to be an important threshold for extensive glaciation of continents in the northern hemisphere (DeConto et al., 2008). Colour-coded horizontal dashed lines in F are averages of equivalent Holocene-aged SST data from the same site. A modern SST value is highlighted for Hole 610A since no equivalent Holocene-aged alkenone SST data are available for this site. See Figure 2 and Supplementary Figure S1 for site locations.

Figure 8. Sub-polar North Atlantic dinoflagellate cyst records and their schematic interpretation in terms of North Atlantic Current (NAC) evolution during MIS M2: (Ai) abundance of dinoflagellate cyst *Operculodinium centrocarpum* (De Schepper et al., 2009; De Schepper et al., 2013), with increase numbers taken to indicate the presence of the NAC over a study site (De Schepper et al., 2013), at DSDP Site 610 and IODP Site U1308, (Aii) and at Site U1313 (De Schepper et al., 2013). (Aii) Globally representative benthic $\delta^{18}O$ stack the LR04 (grey; Lisiecki and Raymo, 2005) and benthic $\delta^{18}O$ from North Atlantic Ocean IODP Site U1313 (black; Bolton et al., 2010). Numbers 1-3 in (A) relate to NAC pathway interpretations illustrated in map shown in B-D. The most southerly position for the NAC during MIS M2 shown in map 2 is inferred from peak abundances of *O. centrocarpum* in U1313 sediments during early glacial conditions. A latitudinal position for the NAC in map 3 that is intermediate between the extremes shown in maps 1 and 2 is based on low abundances of *O. centrocarpum* in both U1313 and 610A/U1308 sediments during full glacial MIS M2.

1299 Table 1. Average values of water mass proxy data from Site 1267 (U1313) during

1300 target glacials (G) and associated interglacials (IG), as well as average IG-G change.

	Marine Isotope Stage average*				**IG-G difference**		
MIS	**ε_{Nd}**	**$\delta^{13}C$**	**$[CO_3^2]$**		**$\Delta\varepsilon_{Nd}$**	**$\Delta\delta^{13}C$**	**$\Delta[CO_3^2]$**
MG1	-11.03 (-11.92)	+0.85 (0.80)	92.7	**MG1-M2**	+1.09 (+0.70)	-0.46 (-0.20)	-0.5
M2	-9.95 (-11.22)	+0.39 (0.59)	92.1				
M1	-11.04 (-11.60)	+0.79 (0.83)	103.1	**M1-M2**	-1.10 (-0.37)	+0.40 (+0.23)	11
101	-11.18 (-12.55)	+0.55 (0.88)	108.1	**101-100**	-1.87 (+1.84)	-0.41 (-0.76)	22.2
100	-9.31 (-10.71)	+0.14 (0.12)	85.8				
99	-10.04 (-11.88)	+0.30 (0.89)	102.1	**99-100**	-0.73 (-1.17)	+0.16 (+0.76)	16.2
MIS 2	-9.57 (-11.48)	+0.05 (0.19)	82.3				
MIS 1	-10.74 (-13.98)	+0.57 (0.90)	92.9	**1-2**	-1.17 (-1.84)	+0.52 (+0.55)	10.6

1301 *determined using LR04 definitions of MIS boundaries (Lisiecki and Raymo, 2005) apart from for

1302 MIS M1 (where we use 3238-3285 ka) and MIS M2 (where we use 3285-3312 ka).

Figure 1

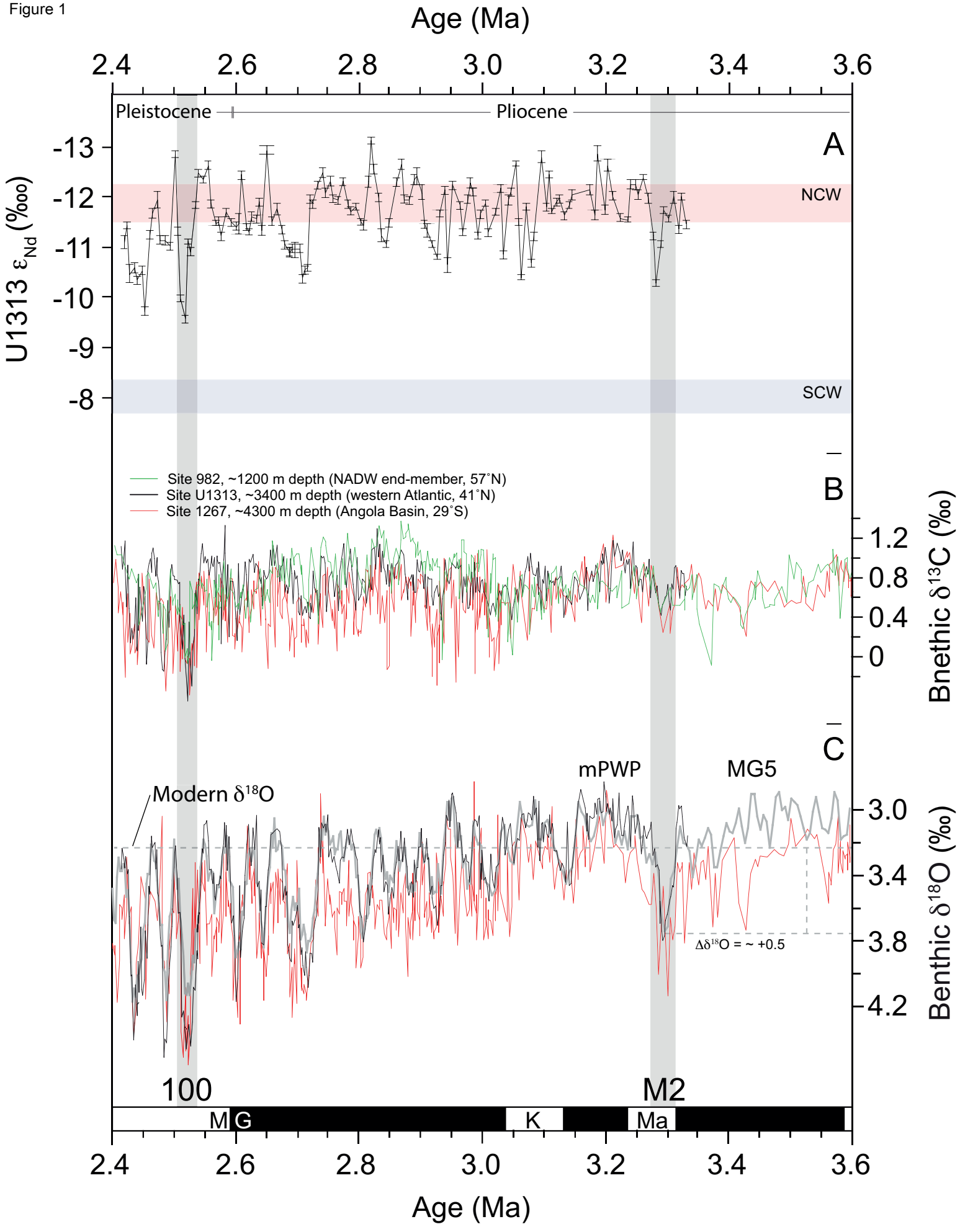
Age (Ma)
2.4
2.6
2.8
3.0
3.2
3.4
3.6
Pleistocene
Pliocene
A
NCW
SCW
U1313 ε_Nd (‰)
-13
-12
-11
-10
-9
-8
B
Site 982, ~1200 m depth (NADW end-member, 57˚N)
Site U1313, ~3400 m depth (western Atlantic, 41˚N)
Site 1267, ~4300 m depth (Angola Basin, 29˚S)
Bnethic δ13C (‰)
1.2
0.8
0.4
0
C
Modern δ18O
mPWP
MG5
Δδ18O = ~ +0.5
Benthic δ18O (‰)
3.0
3.4
3.8
4.2
100
M2
M
G
K
Ma
Age (Ma)

Figure 2

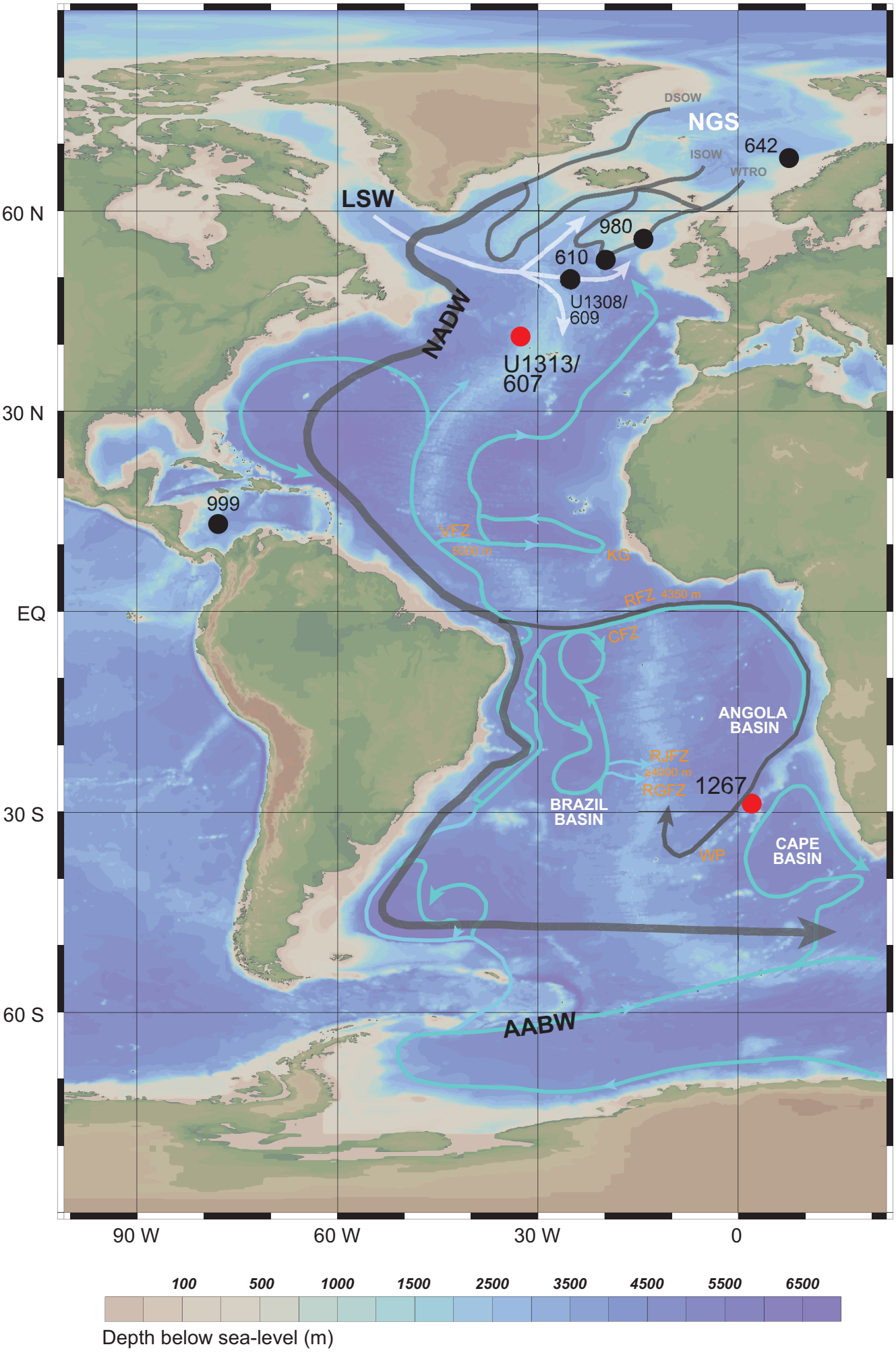
DSOW
NGS
642
ISOW
WTRO
LSW
980
610
U1308/
609
NADW
U1313/
607
999
VFZ
5000 m
KG
RFZ 4350 m
CFZ
ANGOLA
BASIN
RJFZ
≥4000 m
RGFZ
1267
BRAZIL
BASIN
WP
CAPE
BASIN
AABW
60 N
30 N
EQ
30 S
60 S
90 W
60 W
30 W
0
100
500
1000
1500
2500
3500
4500
5500
6500
Depth below sea-level (m)

Figure 3

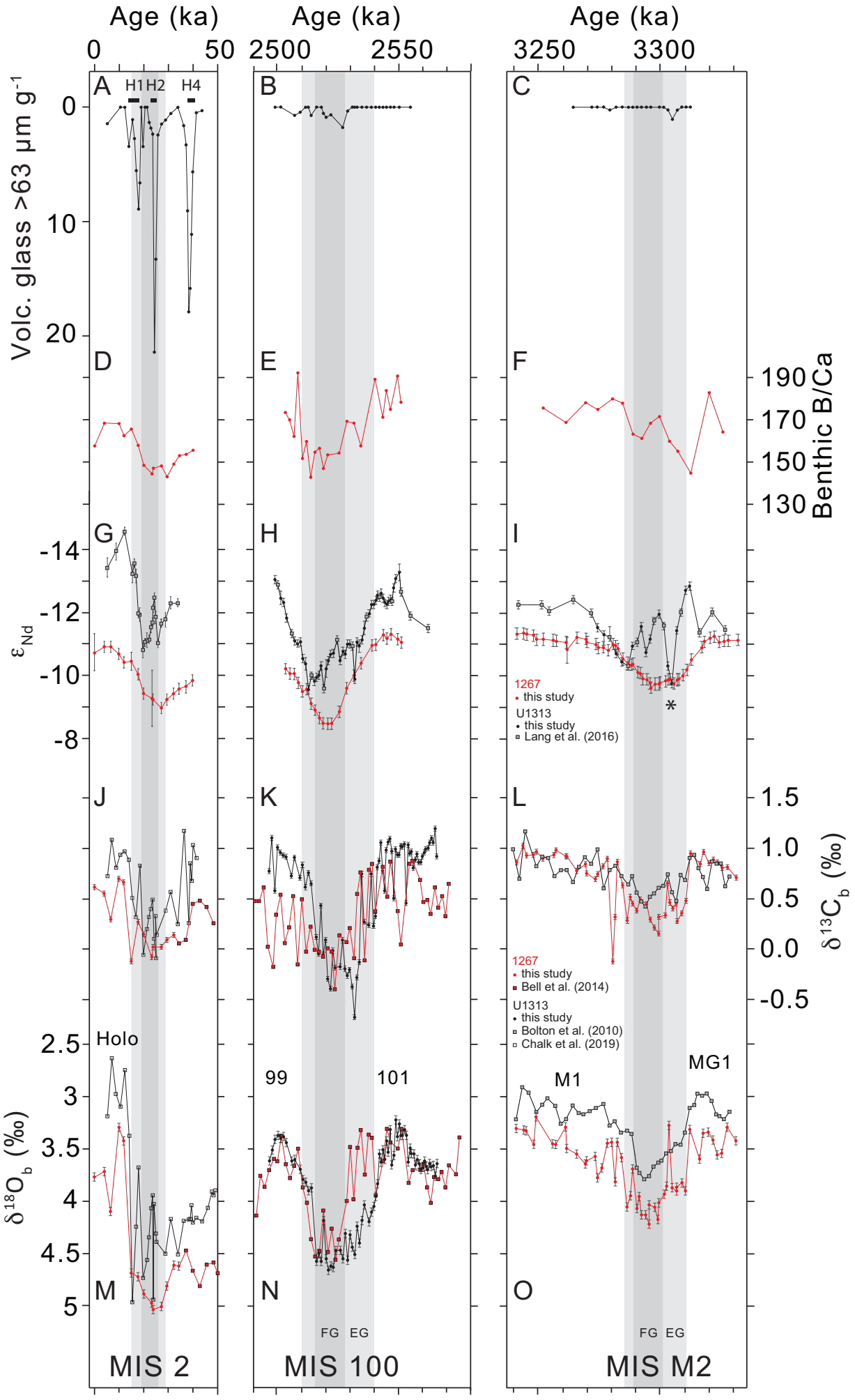
Age (ka)
0
50
2500
2550
3250
3300
A
H1
H2
H4
B
C
Volc. glass >63 µm g-1
0
10
20
D
E
F
190
170
150
130
Benthic B/Ca
G
H
I
-14
-12
-10
-8
εNd
1267
this study
U1313
this study
Lang et al. (2016)
*
J
K
L
1.5
1.0
0.5
0.0
-0.5
δ13Cb (‰)
1267
this study
Bell et al. (2014)
U1313
this study
Bolton et al. (2010)
Chalk et al. (2019)
Holo
2.5
3
3.5
4
4.5
5
δ18Ob (‰)
99
101
M1
MG1
M
N
O
FG
EG
MIS 2
MIS 100
MIS M2

Figure 4

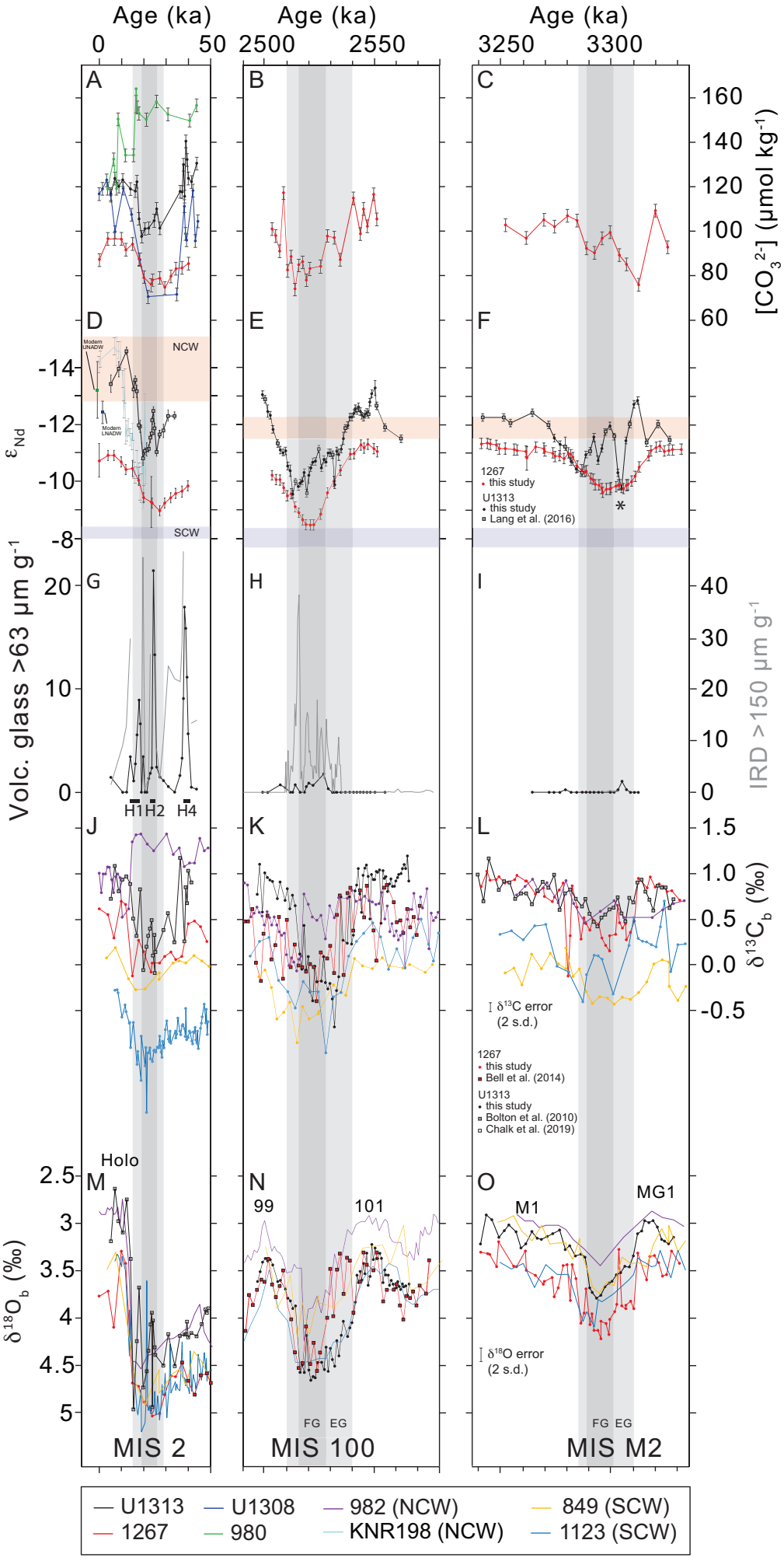
Age (ka)
0
50
2500
2550
3250
3300
A
B
C
D
E
F
G
H
I
J
K
L
M
N
O
160
140
120
100
80
60
[CO3 2-] (µmol kg-1)
NCW
SCW
Modern LNADW
Modern LNADW
-14
-12
-10
-8
εNd
1267
this study
U1313
this study
Lang et al. (2016)
*
20
10
0
Volc. glass >63 µm g-1
H1
H2
H4
40
30
20
10
0
IRD >150 µm g-1
1.5
1.0
0.5
0.0
-0.5
δ13Cb (‰)
δ13C error
(2 s.d.)
1267
this study
Bell et al. (2014)
U1313
this study
Bolton et al. (2010)
Chalk et al. (2019)
Holo
2.5
3
3.5
4
4.5
5
δ18Ob (‰)
99
101
M1
MG1
δ18O error
(2 s.d.)
FG
EG
FG
EG
MIS 2
MIS 100
MIS M2
U1313
1267
U1308
980
982 (NCW)
KNR198 (NCW)
849 (SCW)
1123 (SCW)

Figure 5

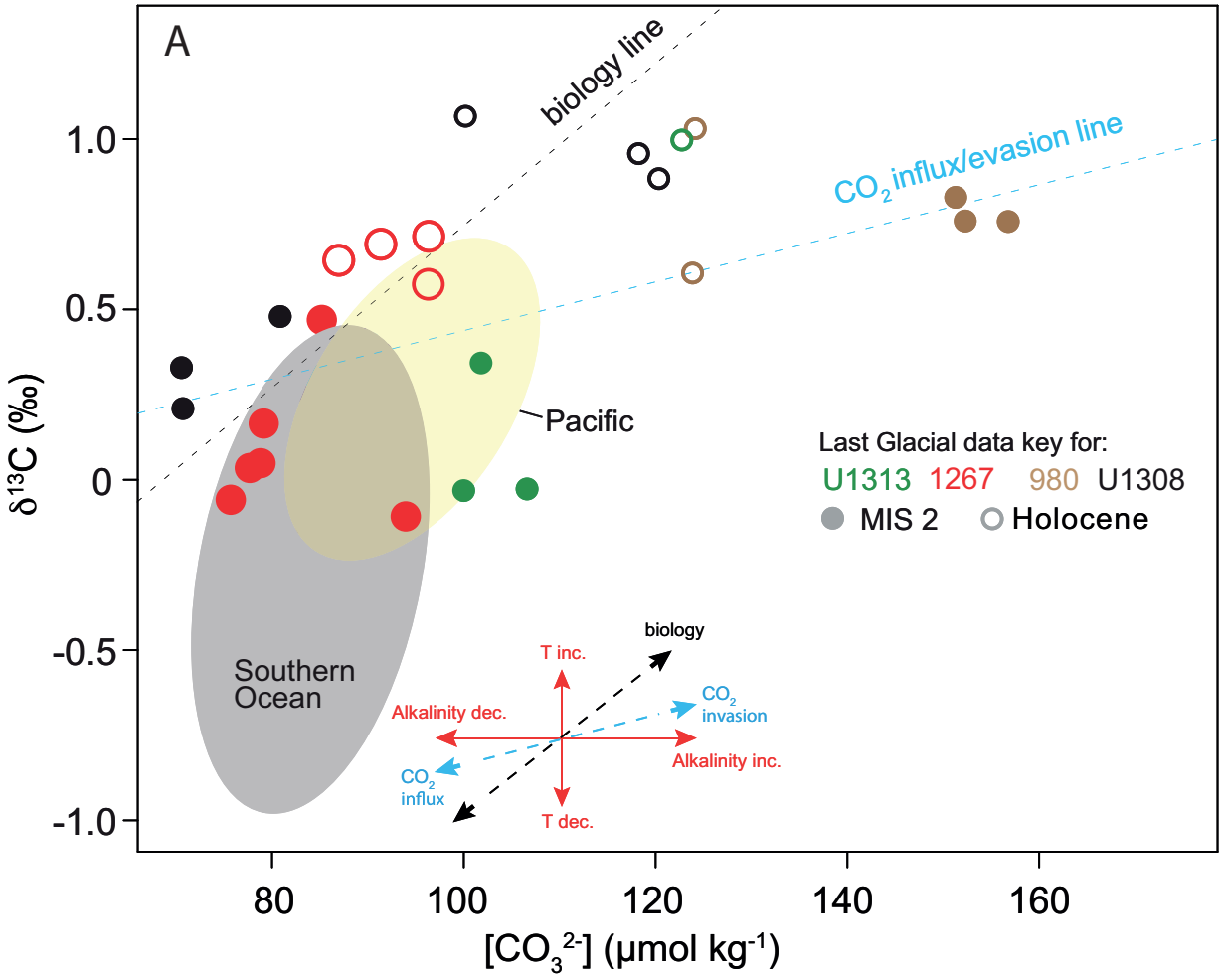
A
biology line
CO2 influx/evasion line
Pacific
Southern Ocean
Last Glacial data key for:
U1313 1267 980 U1308
MIS 2 Holocene
biology
T inc.
CO2 invasion
Alkalinity dec.
Alkalinity inc.
CO2 influx
T dec.
δ13C (‰)
[CO3 2-] (µmol kg-1)
1.0
0.5
0
-0.5
-1.0
80
100
120
140
160

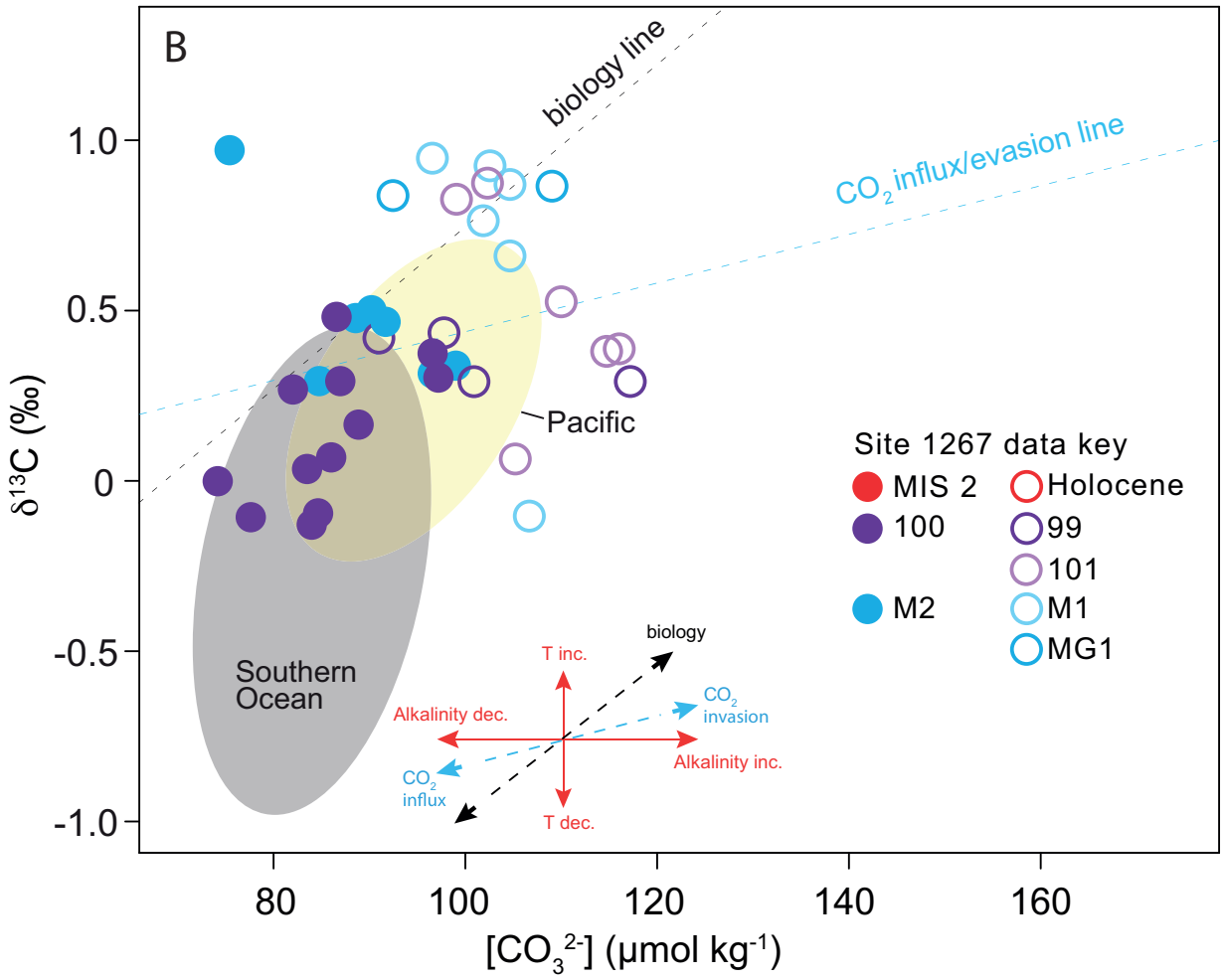
B
biology line
CO2 influx/evasion line
Pacific
Southern Ocean
Site 1267 data key
MIS 2
Holocene
100
99
101
M2
M1
MG1
biology
T inc.
CO2 invasion
Alkalinity dec.
Alkalinity inc.
CO2 influx
T dec.
δ13C (‰)
[CO3 2-] (µmol kg-1)
1.0
0.5
0
-0.5
-1.0
80
100
120
140
160

Figure 6

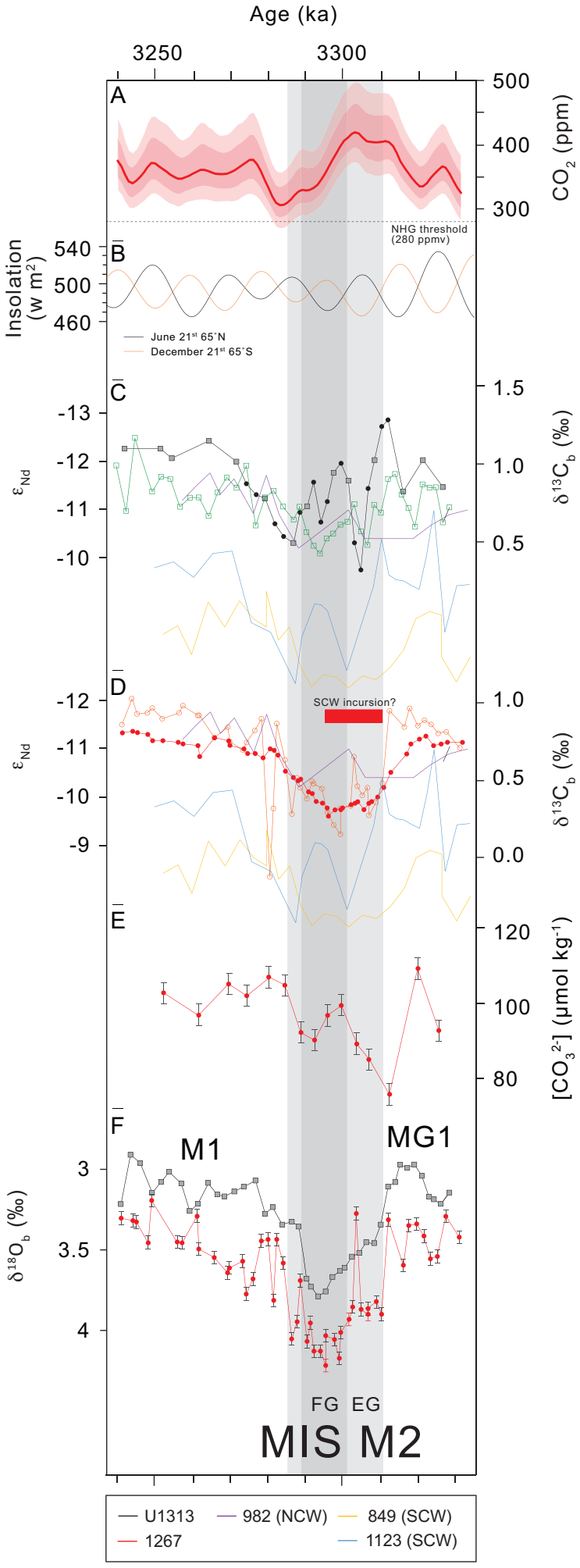
Age (ka)
3250
3300
A
500
400
300
CO_2 (ppm)
NHG threshold
(280 ppmv)
B
Insolation
(w m^2)
540
500
460
June 21st 65°N
December 21st 65°S
C
-13
-12
-11
-10
ε_{Nd}
1.5
1.0
0.5
$\delta^{13}C_b$ (‰)
D
SCW incursion?
-12
-11
-10
-9
ε_{Nd}
1.0
0.5
0.0
$\delta^{13}C_b$ (‰)
E
120
100
80
$[CO_3^{2-}]$ (µmol kg^{-1})
F
M1
MG1
3
3.5
4
$\delta^{18}O_b$ (‰)
FG
EG
MIS M2
U1313
982 (NCW)
849 (SCW)
1267
1123 (SCW)

Figure 7

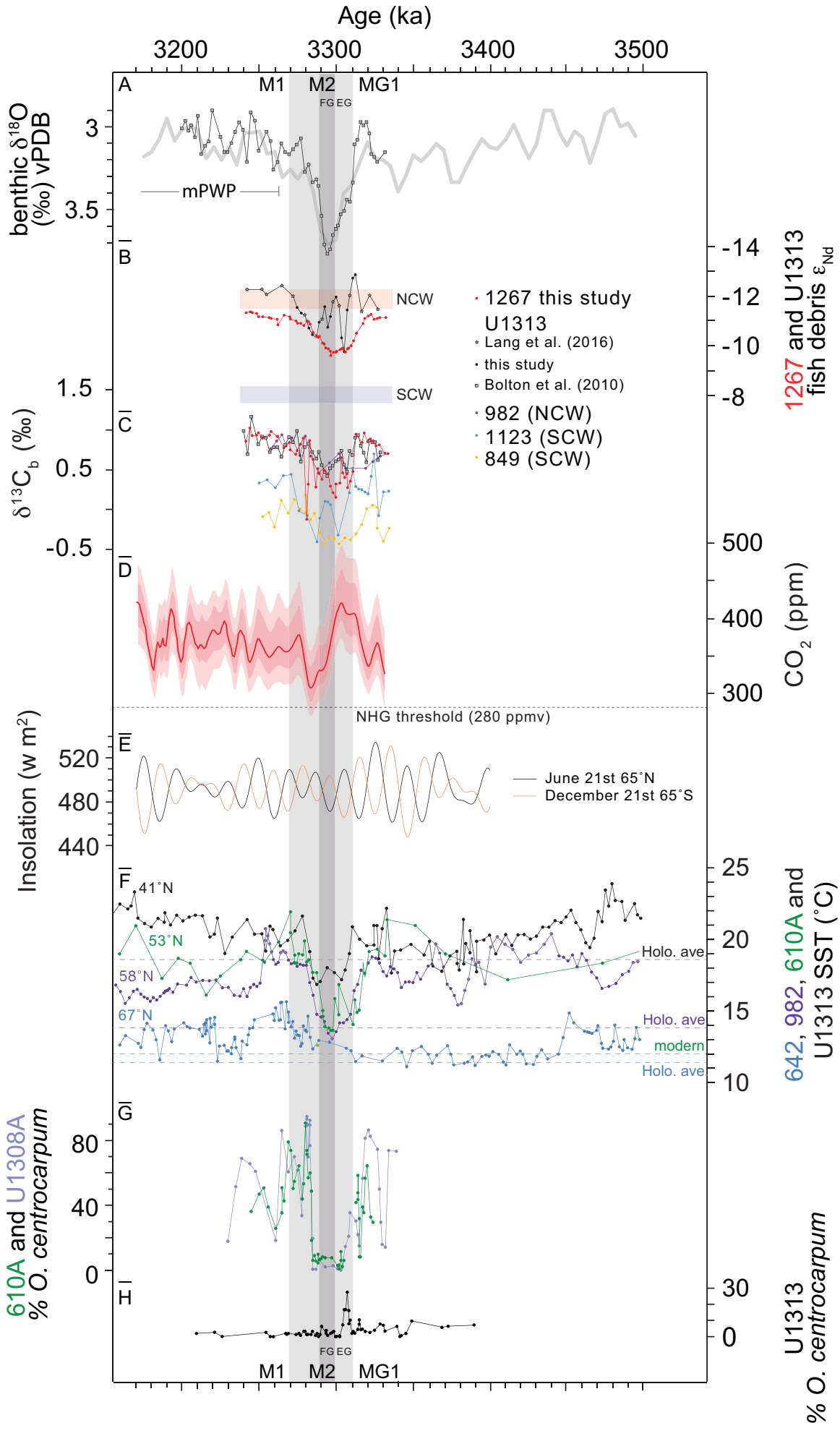
Age (ka)
3200
3300
3400
3500
A
M1
M2
MG1
FG EG
benthic δ18O (‰) vPDB
3
3.5
mPWP
B
NCW
SCW
1267 this study
U1313
Lang et al. (2016)
this study
Bolton et al. (2010)
982 (NCW)
1123 (SCW)
849 (SCW)
1267 and U1313 fish debris εNd
-14
-12
-10
-8
δ13Cb (‰)
1.5
0.5
-0.5
C
D
500
400
300
CO2 (ppm)
NHG threshold (280 ppmv)
Insolation (w m2)
520
480
440
E
June 21st 65˚N
December 21st 65˚S
F
41˚N
53˚N
58˚N
67˚N
Holo. ave
Holo. ave
modern
Holo. ave
642, 982, 610A and U1313 SST (˚C)
25
20
15
10
610A and U1308A % O. centrocarpum
G
80
40
0
H
30
0
U1313 % O. centrocarpum
FG EG
M1
M2
MG1

Figure 8

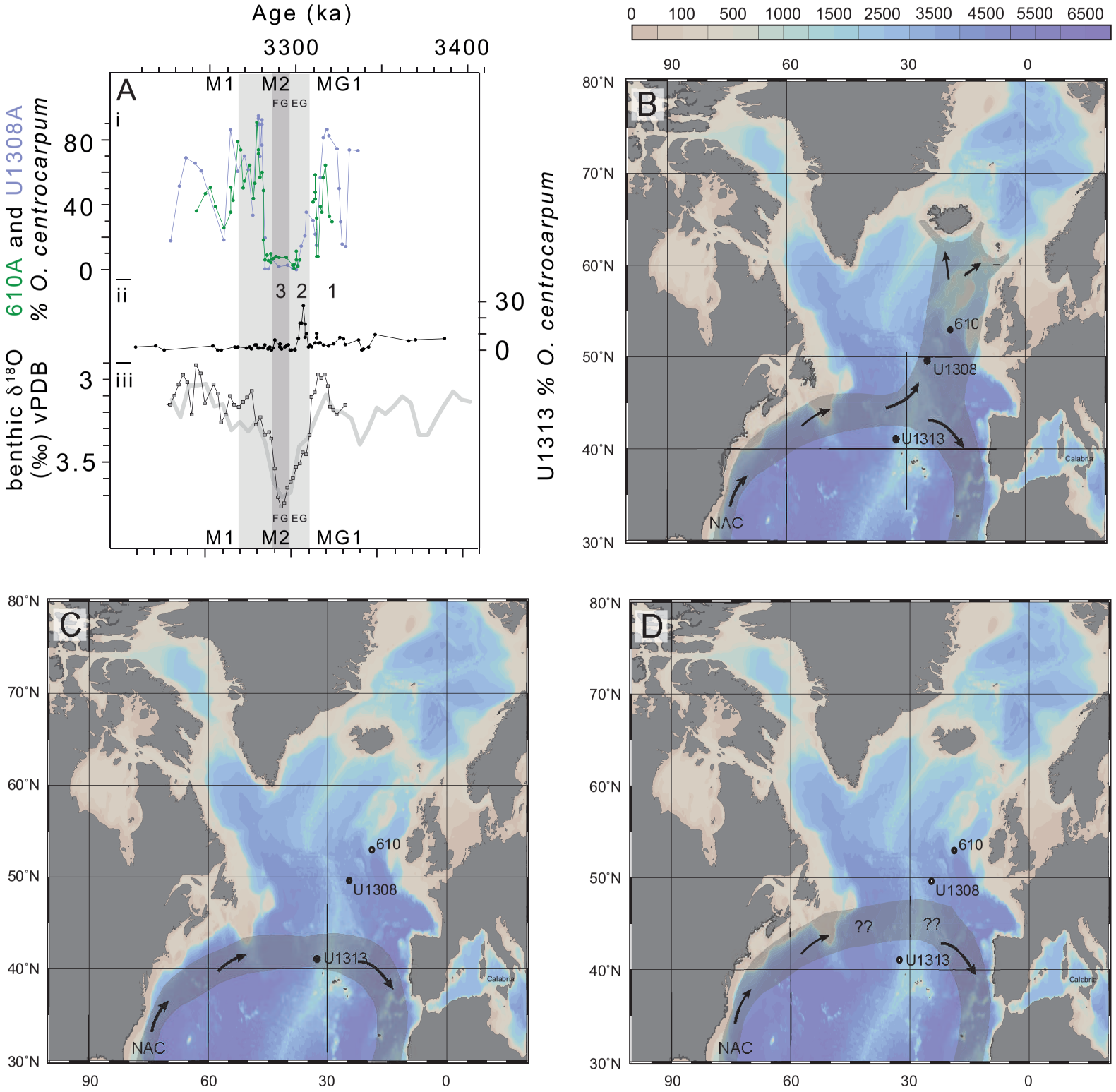
Age (ka)
3300
3400
A
M1
M2
MG1
FG
EG
i
ii
iii
3 2 1
80
40
0
3
3.5
30
0
610A and U1308A % O. centrocarpum
benthic δ18O (‰) vPDB
U1313 % O. centrocarpum
0 100 500 1000 1500 2500 3500 4500 5500 6500
90 60 30 0
B
C
D
80°N
70°N
60°N
50°N
40°N
30°N
610
U1308
U1313
NAC
Calabria
??

Kirby et al.: On climate and abyssal circulation in the Atlantic Ocean during late Pliocene marine isotope stage M2, ~3.3 million years ago

Conflict of interest statement: The authors declare that they have no competing financial interests or personal relationships that influenced the work reported in this paper

Author Contributions: N.K generated the Site 1267 data and contributed to manuscript writing; I.B. designed the study, supervised N.K. in data generation and wrote the manuscript; A.B generated the Site U1313 stable isotope data for MIS 100 and contributed to manuscript writing; T.B.C. supervised R.L.P in generating the Site 1267 benthic B/Ca data and contributed to the ideas presented and to manuscript writing; R.L.P generated a subset of the Site 1267 data; A.J.C. supervised N.K. and R.L.P in data generation, contributed to the ideas presented and to manuscript writing; V.E.T. supervised N.K. and R.L.P. in data generation, generated the volcanic glass count data and contributed to manuscript writing; J.A.M helped to generate the Nd isotope data; G.L.F. contributed to the ideas presented and manuscript writing; M.E.R. contributed to the ideas presented and manuscript writing; D.K. contributed samples and to the ideas presented and manuscript writing; D.B.B contributed samples and to manuscript writing; P.A.W. designed the study, supervised N.K. in data generation, co-wrote the manuscript with I.B.